NATURAL RESOURCES

TSUNAMI HAZARD MAPS OF THE OLYMPIC PENINSULA—MODEL RESULTS FROM AN EXTENDED L1 Mw 9.0 CASCADIA SUBDUCTION ZONE MEGATHRUST EARTHQUAKE SCENARIO

by Alexander Dolcimascolo, Daniel W. Eungard, Corina Allen, Randall J. LeVeque, Loyce M. Adams, Diego Arcas, Vasily V. Titov, Frank I. González, Christopher Moore, Carrie E. Garrison-Laney, and Timothy J. Walsh

WASHINGTON
GEOLOGICAL SURVEY
Map Series 2022-01
January 2022

INTERNALLY REVIEWED

WASHINGTON STATE DEPARTMENT OF
NATURAL RESOURCES
WASHINGTON GEOLOGICAL SURVEY

TSUNAMI HAZARD MAPS OF THE OLYMPIC PENINSULA—MODEL RESULTS FROM AN EXTENDED L1 Mw 9.0 CASCADIA SUBDUCTION ZONE MEGATHRUST EARTHQUAKE SCENARIO

by Alexander Dolcimascolo, Daniel W. Eungard, Corina Allen, Randall J. LeVeque, Loyce M. Adams, Diego Arcas, Vasily V. Titov, Frank I. González, Christopher Moore, Carrie E. Garrison-Laney, and Timothy J. Walsh

WASHINGTON
GEOLOGICAL SURVEY
Map Series 2022-01
January 2022

This publication has been subject to an iterative technical review process by at least one Survey geologist who is not an author. This publication has also been subject to an iterative review process with Survey editors and cartographers and has been formatted by Survey staff.

WASHINGTON STATE DEPARTMENT OF
NATURAL RESOURCES
WASHINGTON GEOLOGICAL SURVEY

DISCLAIMER

Neither the State of Washington, nor any agency thereof, nor any of their employees, makes any warranty, express or implied, or assumes any legal liability or responsibility for the accuracy, completeness, or usefulness of any information, apparatus, product, or process disclosed, or represents that its use would not infringe privately owned rights. Reference herein to any specific commercial product, process, or service by trade name, trademark, manufacturer, or otherwise, does not necessarily constitute or imply its endorsement, recommendation, or favoring by the State of Washington or any agency thereof. The views and opinions of authors expressed herein do not necessarily state or reflect those of the State of Washington or any agency thereof.

This map product has been subjected to an iterative internal review process by agency geologists, cartographers, and editors and meets Map Series standards as defined by the Washington Geological Survey.

INDEMNIFICATION

This item was partially funded by the National Oceanic and Atmospheric Administration (NOAA) award no. NA20NWS4670068 to the Washington Geological Survey. This does not constitute an endorsement by NOAA.

Washington State Department of Natural Resources
Washington Geological Survey

Mailing Address:
1111 Washington St. SE
MS 47007
Olympia, WA 98504-7007

Street Address:
Natural Resources Bldg, Rm 148
1111 Washington St SE
Olympia, WA 98501

Phone: 360-902-1450
Fax: 360-902-1785
Email: geology@dnr.wa.gov
Website: http://www.dnr.wa.gov/geology

Publications and Maps:
www.dnr.wa.gov/programs-and-services/geology/publications-and-data/publications-and-maps

Washington Geology Library Searchable Catalog:
www.dnr.wa.gov/programs-and-services/geology/washington-geology-library

Suggested Citation: Dolcimascolo, Alexander; Eungard, D. W.; Allen, Corina; LeVeque, R. J.; Adams, L. M.; Arcas, Diego; Titov, V. V.; González, F. I.; Moore, Christopher; Garrison-Laney, C. E.; Walsh, T. J., 2022, Tsunami hazard maps of the Olympic Peninsula—Model results from an extended L1 Mw 9.0 Cascadia subduction zone megathrust earthquake scenario: Washington Geological Survey Map Series 2022-01, 14 sheets, scale 1:48,000, 21 p. text. [https://fortress.wa.gov/dnr/geologydata/tsunami_hazard_maps/ger_ms2022-01_tsunami_hazard_olympic_peninsula.zip]

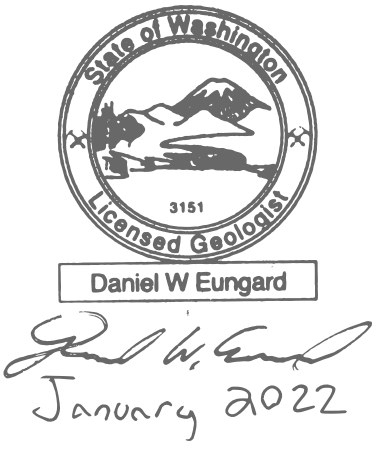

Contents

FIGURES

TABLES

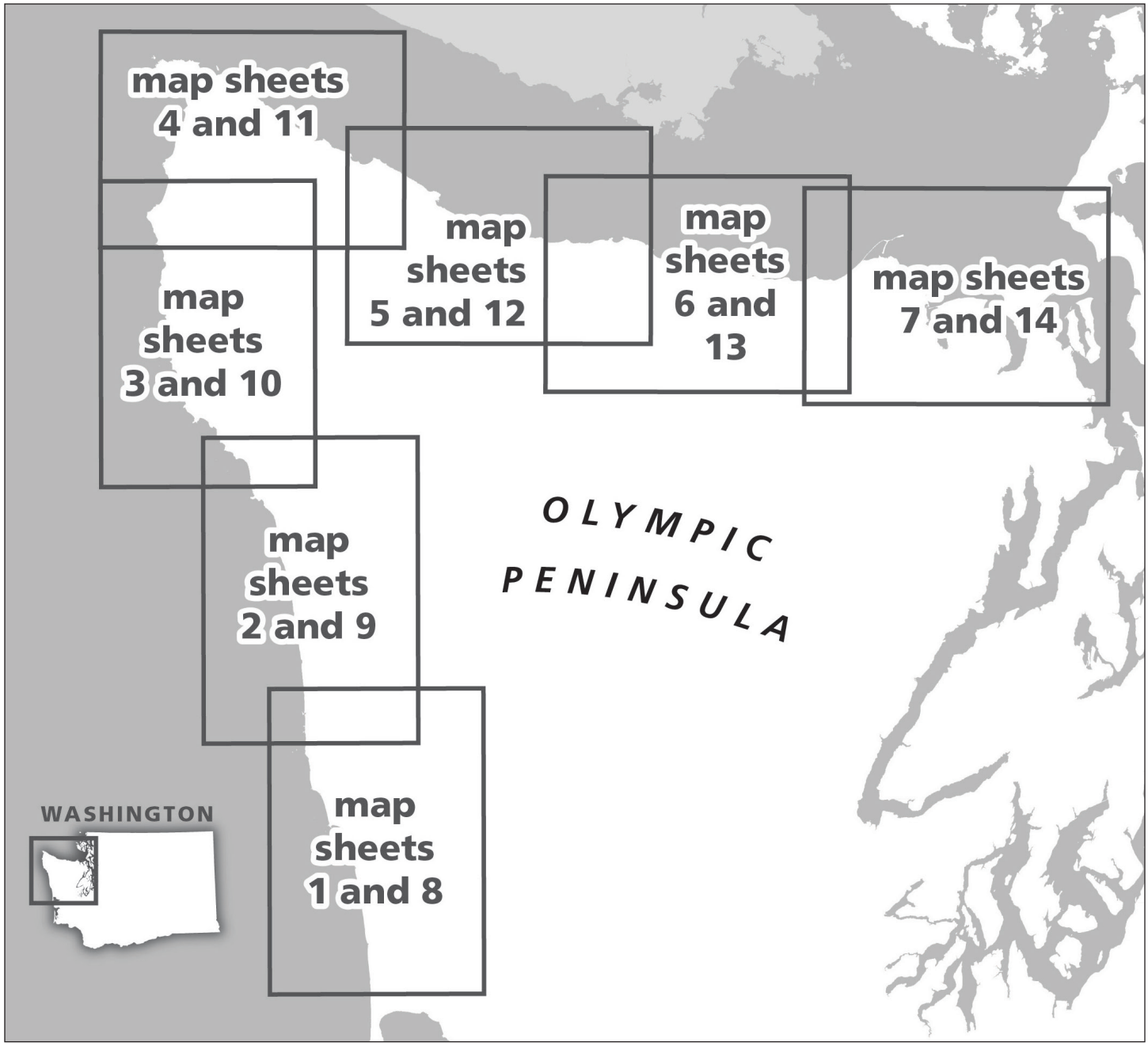

MAP SHEET

Map Sheet 1. Detailed tsunami inundation of the Olympic Peninsula—Quinault
Map Sheet 2. Detailed tsunami inundation of the Olympic Peninsula—Hoh
Map Sheet 3. Detailed tsunami inundation of the Olympic Peninsula—Ozette
Map Sheet 4. Detailed tsunami inundation of the Olympic Peninsula—Neah Bay
Map Sheet 5. Detailed tsunami inundation of the Olympic Peninsula—Lake Crescent
Map Sheet 6. Detailed tsunami inundation of the Olympic Peninsula—Port Angeles
Map Sheet 7. Detailed tsunami inundation of the Olympic Peninsula—Dungeness
Map Sheet 8. Tsunami maximum current speed of the Olympic Peninsula—Quinault
Map Sheet 9. Tsunami maximum current speed of the Olympic Peninsula—Hoh
Map Sheet 10. Tsunami maximum current speed of the Olympic Peninsula—Ozette
Map Sheet 11. Tsunami maximum current speed of the Olympic Peninsula—Neah Bay
Map Sheet 12. Tsunami maximum current speed of the Olympic Peninsula—Lake Crescent
Map Sheet 13. Tsunami maximum current speed of the Olympic Peninsula—Port Angeles
Map Sheet 14. Tsunami maximum current speed of the Olympic Peninsula—Dungeness

Tsunami Hazard Maps of the Olympic Peninsula—Model Results from an Extended L1 Mw 9.0 Cascadia Subduction Zone Megathrust Earthquake Scenario

by Alexander Dolcimascolo[1], Daniel W. Eungard[1], Corina Allen[1], Randall J. LeVeque[2], Loyce M. Adams[2], Diego Arcas[3], Vasily V. Titov[3], Frank I. González[4], Christopher Moore[3], Carrie E. Garrison-Laney[5], and Timothy J. Walsh[1]

[1] Washington Geological Survey
1111 Washington St SE
MS 47007
Olympia, WA 98504-7007

[2] Department of Applied Mathematics
4182 W Stevens Way NE
University of Washington
Seattle, WA 98195-3925

[3] National Oceanic and Atmospheric Administration
Pacific Marine Environmental Laboratory
7600 Sand Point Way NE
Seattle, WA 98115-6349

[4] Department of Earth and Space Sciences
University of Washington
4000 15th Ave NE
Seattle, WA 98195-1310

[5] Washington Sea Grant
University of Washington
3716 Brooklyn Ave NE
Seattle, WA 98105-6716

ABSTRACT

We present new tsunami inundation modeling for the Olympic Peninsula in northwestern Washington to encourage hazard planning and increase community resilience. This modeling uses a simulated magnitude 9.0 earthquake along the Cascadia subduction zone, producing a tsunami that is unlikely to be exceeded in the next great earthquake. The simulated earthquake fault geometry assumes a full-length rupture of Cascadia that spans ~775 mi from northern California to just north of Vancouver Island, Canada. Scientists inferred that this scenario encompasses ~95 percent of the variability of Cascadia tsunami simulations. This seismic scenario assumes that all coastal elevations in this study area will drop from coseismic subsidence. Earthquake shaking would be felt in all locations within the study area prior to the arrival of the tsunami, though subsidence impacts would be greatest closer to the subduction zone. The first modeled rising tsunami wave arrives at La Push within 10 minutes from the start of the earthquake shaking. However, localized flooding could occur within minutes of the earthquake due to subsidence of the land relative to global sea level. The crest of the first modeled tsunami wave exceeds 30 ft (9 m) and reaches many locations along the Pacific coast within ~30 minutes. Flooding depths on land also reach or exceed 60 ft (18 m) along most Pacific coastline beaches and campgrounds. The first modeled rising wave of the tsunami also travels into the Strait of Juan de Fuca and reaches Port Angeles in ~1 hour with a wave amplitude of ~20 ft (6 m). There is limited time to issue official tsunami warnings and any felt earthquake shaking should act as an immediate warning. Fast-moving currents from the tsunami waves locally exceed 9 knots off Washington's Pacific coastline and within some areas in the Strait of Juan de Fuca, presenting a significant navigational hazard to the maritime community. Tsunami wave inundation would likely continue over 8 hours and remain hazardous to maritime operations for more than 24 hours. This study is limited in that modeling does not account for tide stage, tidal currents, earthquake-induced landslides, seiches, liquefaction, or minor topographic changes that would locally modify the effects of tsunami waves. In addition, there are many assumptions associated with the scenario earthquake and its probability of occurrence modeled here. Due to these limitations, this modeling may not be suitable for site-specific tsunami inundation assessment or for determining effects on the built environment. Instead, we recommend using this modeling as a tool to assist with emergency preparations and evacuation planning prior to a Cascadia subduction zone event or to determine locations where a tsunami vertical evacuation refuge would be appropriate.

INTRODUCTION

The Cascadia subduction zone (CSZ) stretches for about 775 mi along the Pacific Ocean from Cape Mendocino, California to just north of Vancouver Island, Canada. At the CSZ, the Juan de Fuca, Explorer, and Gorda oceanic plates slide beneath the North American continental plate (Fig. 1), generating great earthquakes when built up strain abruptly releases. These earthquakes can produce tsunamis that pose a significant hazard to Washington and possibly to other coastlines in the Pacific Ocean.

Numerous workers found geologic evidence of tsunami deposits attributed to the CSZ in at least 59 localities from northern California to southern Vancouver Island (compiled in Peters and others, 2003). The observed evidence of past seismicity and tsunamis suggests that not all earthquakes generated by the

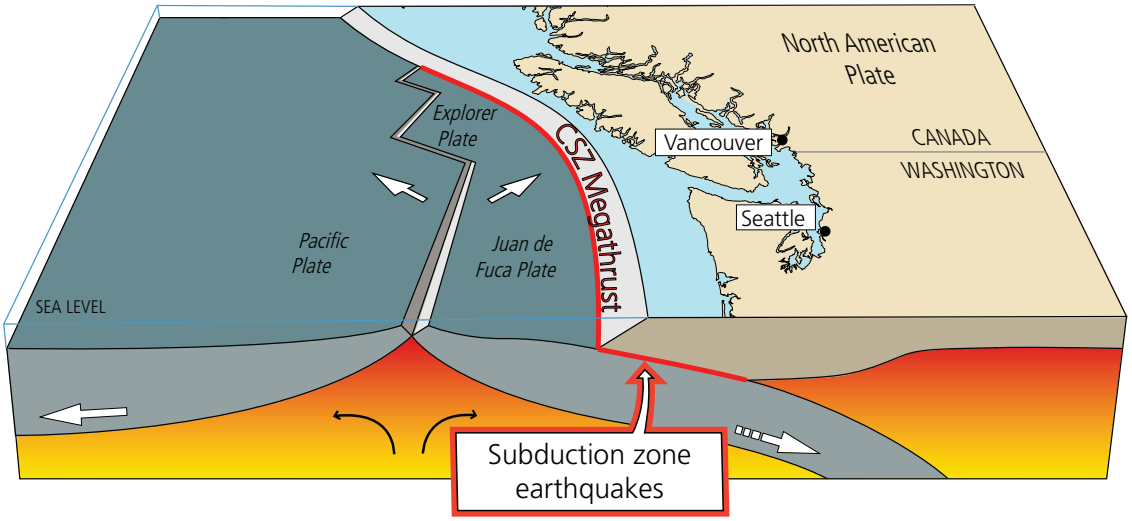

Source	Maximum Size	Average Recurrence Interval	Major Past Earthquakes (Year)
CSZ Megathrust	M 9	500-600 yr	1700

Figure 1. Tectonic overview of part of the Cascadia subduction zone (CSZ). The red line indicates the subduction zone interface (where the Juan de Fuca, Explorer, and Gorda [not pictured] oceanic plates subduct under the overriding North American plate) that may host a megathrust earthquake. Strain builds up along this interface, generating earthquakes when it releases. The release of strain deforms the seafloor and represents the source of tsunamis for the CSZ (Figure modified from the USGS).

CSZ are the same. The preserved geologic record both onshore and offshore presents clues that help quantify the history of earthquakes along the CSZ. This information has become crucial for tsunami modeling and hazard preparedness, especially after recent events in the Indian Ocean in 2004 and Japan in 2011, where the hazard was underestimated. The multitude of geologic findings (see *Appendix A* for a fuller discussion) and the recent catastrophic tsunami events in other parts of the world have now encouraged tsunami modelers and preparedness efforts to focus on less likely, less frequent, though more damaging hazard scenarios than were previously considered.

Research over the last few decades illustrating the impacts of CSZ earthquakes and tsunamis along the shorelines of British Columbia (Hutchinson and Clague, 2017), Washington (Atwater, 1992; Atwater and others, 1995), Oregon (Kelsey and others, 2005), and northern California (Padgett and others, 2021) has demonstrated that these events will leave little time for evacuation. A key component of tsunami hazard assessment, and the first step in developing evacuation plans, is to identify areas subject to tsunami inundation (flooding caused by tsunami waves). This study focuses on modeling maximum tsunami inundation and current speeds for Washington's northwest Pacific coast and the Strait of Juan de Fuca on the Olympic Peninsula (Fig. 2). Our study results are based on a scenario earthquake and resultant tsunami, in which the tsunami is estimated to encompass 95 percent of the maximum inundation modeled in a suite of hypothetical CSZ tsunami scenarios (Witter and others, 2011). This scenario produces a tsunami that is unlikely to be exceeded in the next CSZ event.

TSUNAMI SOURCE MODELS

In this study, we use the "Extended L1" earthquake scenario to model the impacts of a CSZ tsunami for the Olympic Peninsula. Previous CSZ tsunami modeling in Washington over the past 21 years used other models that represent different scenarios (Table 1). These include the "1A" scenario (Myers and others, 1999; Priest and others, 1997) and the "L1" scenario (Witter and others, 2011; 2013). Researchers based the 1A scenario on the last CSZ event in 1700, but subsequent research suggested that there were larger events than the event in the year 1700 (Witter and others, 2011; Goldfinger and others, 2012; Witter and others, 2013). The next model scenario was the L1 scenario from Witter and others (2011, 2013), which inferred higher variability in both the amount of slip and slip distribution from the paleotsunami record than the 1A scenario, producing a larger tsunami. Specifically, the L1 scenario has a maximum amount of slip of 88.6 ft (27 m) and partitions this slip to a splay fault (a thrust fault in the accretionary wedge) that has an approximate 30-degree landward dip (Fig 3). This rupture geometry provides more conservative estimates compared to previous tsunami modeling that used the 1A scenario, which assumed a lesser amount of maximum slip of 62 ft (19 m) that was placed solely within the subduction zone interface without intersecting the seafloor. Thus, the splay fault included in the L1 scenario results in a much higher, narrower area of uplift compared to the rupture geometry of the 1A scenario, which dips much more shallowly and reaches farther seaward than the splay fault. Recently, the National Oceanic and Atmospheric Administration (NOAA) Center for Tsunami Research at the Pacific Marine Environmental Laboratory (PMEL) modified the original L1 scenario to account

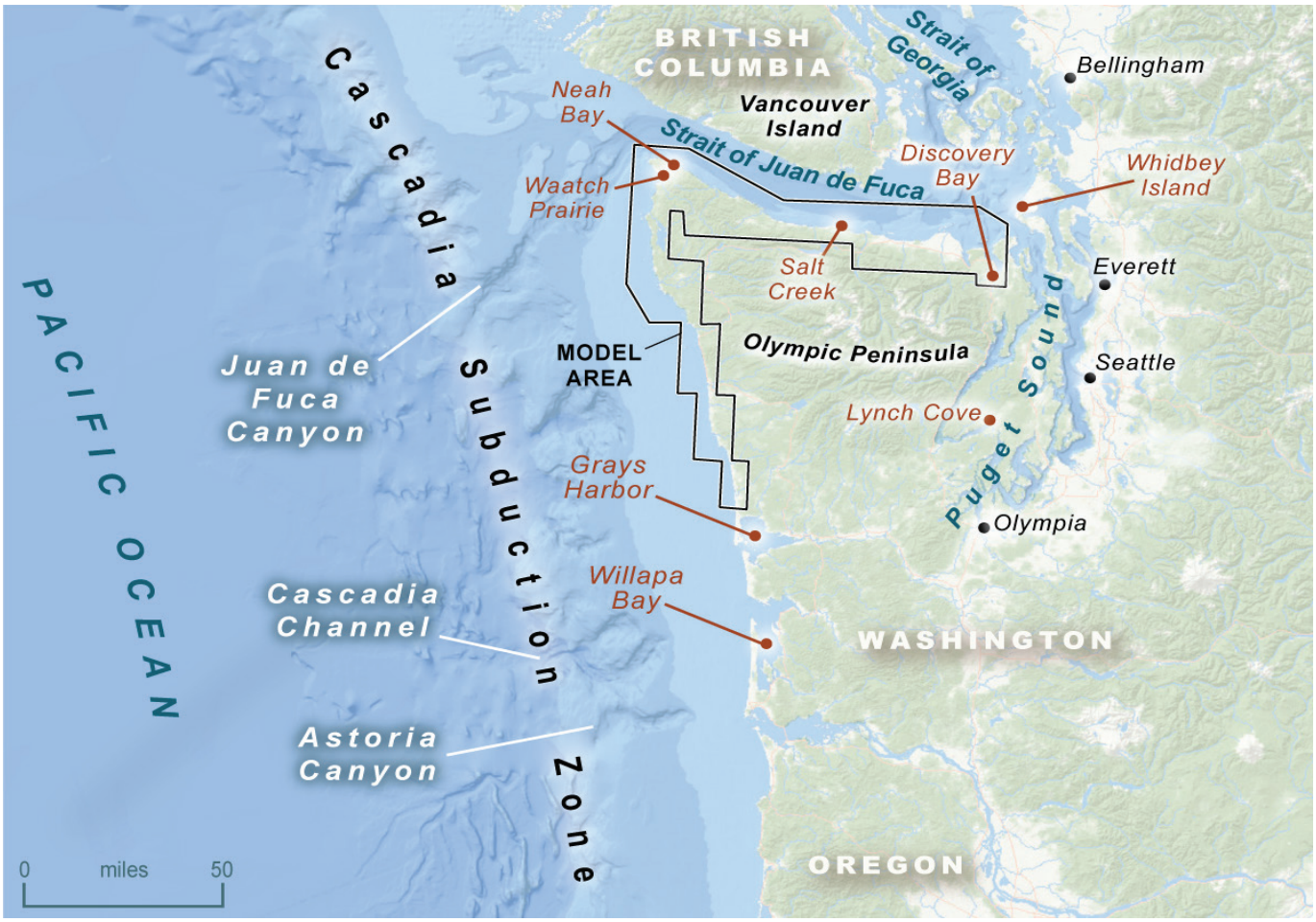

Figure 2. Map of the modeled area, showing the Cascadia subduction zone (CSZ) and major offshore channels. The black polygon outlines the study area of the Olympic Peninsula that corresponds to the included map sheets. Locations marked in red circles contain sedimentary evidence of past tsunamis generated from the CSZ.

Table 1. Published tsunami hazard maps for Washington. CSZ 1A with asperity models incorporate localized areas of offshore uplift.

Location	Reference	Modeled Scenario
Puget Sound and Adjacent Waters	Dolcimascolo and others (2021)	CSZ Extended L1
Anacortes—Bellingham (superseded by Dolcimascolo and others, 2021)	Eungard and others (2018a)	CSZ L1
Port Angeles—Port Townsend (partially superseded by this publication)	Eungard and others (2018b)	CSZ Extended L1
Southwest Washington	Eungard and others (2018c)	CSZ L1
San Juan Islands (partially superseded by Dolcimascolo and others, 2021)	Walsh and others (2016)	CSZ L1
Everett	Walsh and others (2014)	Seattle Fault
Tacoma	Walsh and others (2009)	Tacoma and Seattle Faults
Anacortes—Whidbey Island	Walsh and others (2005)	CSZ 1A
Bellingham	Walsh and others (2004)	CSZ 1A
Neah Bay	Walsh and others (2003a)	CSZ 1A and 1A with asperity
Quileute area	Walsh and others (2003b)	CSZ 1A and 1A with asperity
Seattle	Walsh and others (2003c)	Seattle Fault
Port Angeles	Walsh and others (2002a)	CSZ 1A and 1A with asperity
Port Townsend	Walsh and others (2002b)	CSZ 1A and 1A with asperity
Southern Washington coast	Walsh and others (2000)	CSZ 1A and 1A with asperity

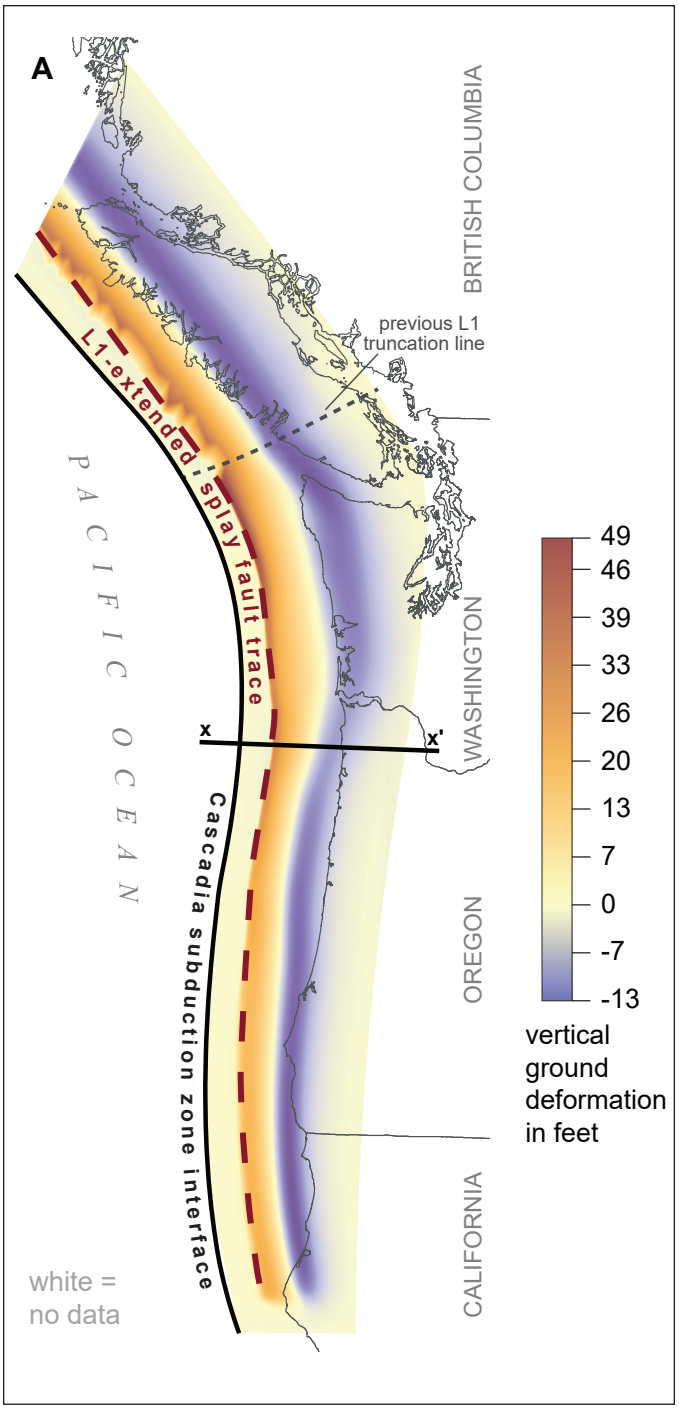

Figure 3. A. Vertical ground deformation for the Extended L1 scenario modified by the NOAA Center for Tsunami Research at PMEL (Gica and Arcas, 2015). **B**. Splay fault model diagram corresponding to the X–X' line in subfigure A.

for an earthquake that ruptures the entire length of the subduction zone from northern California to just north of Vancouver Island, Canada. This Extended L1 scenario now includes the Explorer plate that was omitted in the L1 scenario. Refer to the section 'Comparison of Tsunami Models' in Dolcimascolo and others (2021) for more information on this extension and the comparison between the Extended L1 and L1 source.

Additionally, tsunami modeling presented here on Map Sheets 6 and 13 covers the Port Angeles area that was previously published in Eungard and others (2018b). The newer modeling used here incorporates the updated 2021 topographic and bathymetric elevation data in the Strait of Juan de Fuca whereas Eungard and others (2018b) used the 2015 model. As a result, this publication supersedes the Port Angeles Maps Sheets included in Eungard and others (2018b, see map sheets 1, 3, and 5 therein). The map sheets covering Port Townsend in Eungard and others (2018b) remain unchanged. See Figure 4 for a map of the superseded area.

MODELING APPROACH

The tsunami simulations presented here use two numerical modeling software packages. These packages are the Method of Splitting Tsunami (MOST) and GeoClaw. MOST was developed by PMEL and the University of Southern California (Titov and Synolakis, 1995; 1998; Titov and González, 1997), while GeoClaw is an open-source code (part of the Clawpack software) that was initiated at UW and is still being developed by the UW tsunami modeling group in collaboration with other contributors (Clawpack Development Team, 2021). Both of these packages solve the same set of nonlinear shallow water equations that simulate tsunami generation, propagation, and inundation given specific earthquake and bathymetry inputs. Because this publication is a result of collaboration between the NOAA Center for Tsunami Research at PMEL and the University of Washington's (UW) tsunami modeling group within the Department of Applied Mathematics and UW's Department of Earth & Space Sciences, we used both modeling packages..

Both MOST and GeoClaw have been validated through benchmark tests and are approved by the National Tsunami Hazard Mitigation Program (NTHMP) for use in developing tsunami inundation models (Synolakis and others, 2007; González and others, 2011; Horrillo and others, 2015). To test the practical equivalence between the two software packages, comparative simulations were performed for Bainbridge Island, WA (Titov and others, 2018). The test revealed very close agreement between model results.

The main difference between the software packages is the numerical method employed. The MOST package uses a grid of topographic and bathymetric elevations and calculates a water surface elevation and velocity for each grid cell at specified time intervals. A finite difference numerical scheme solves the nonlinear shallow water equations (Titov and others, 2016). This model also uses a set of three nested grids, referred to as A, B, and C grids, each of which becomes smaller in area and successively finer in resolution as it telescopes into the community of interest.

The GeoClaw package uses a finite volume method that solves the nonlinear shallow water wave equations (George 2006; 2008; George and LeVeque, 2006; Berger and others,

2011; LeVeque and others, 2011; Mandli and others, 2016). The model uses an Adaptive Mesh Refinement (AMR) strategy to calculate water surface elevations and velocities on a fine grid covering the region of interest and records the maximum values over the full simulation time.

Figure 5 illustrates the locations modeled either by MOST or GeoClaw. Since there is a transition from coarse to fine elevation grids for the tsunami models, the edges of the models where these grids transition can introduce erroneous results. We overlap our models to account for these, and opt for the more conservative results (larger maximum values). The vertical reference datum for all tsunami simulation results is the mean high water (MHW) tidal datum. This reference point stays static throughout the simulation by not including changes in the tides over time, leading to more conservative inundation values.

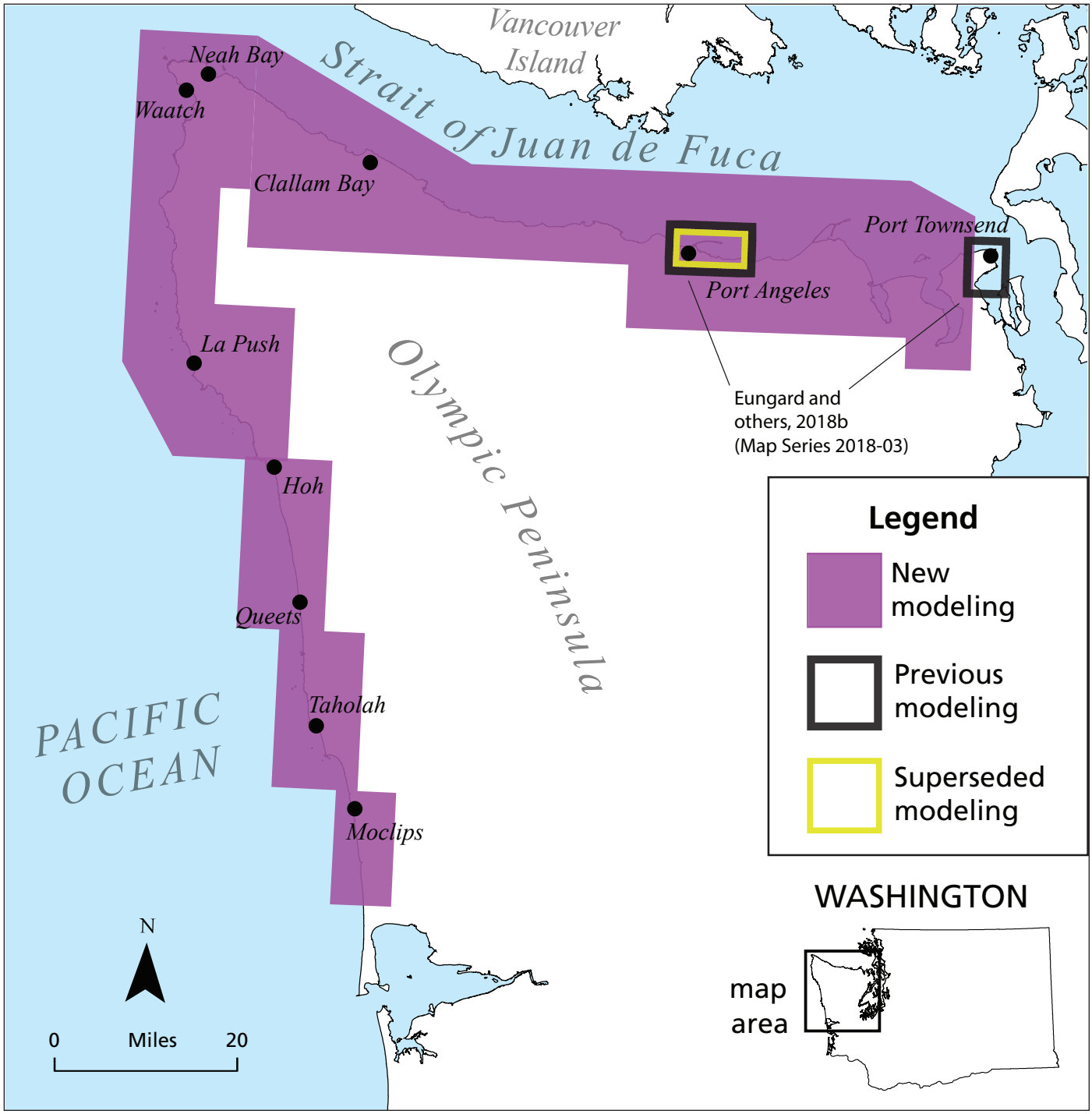

Figure 4. Map of new modeling (purple) compared to areas of previous modeling (black outline). New modeling fully supersedes the Port Angeles region (yellow outline) of Eungard and others (2018b) due to the use of updated topographic and bathymetric elevation data for the Strait of Juan de Fuca. The new modeling does not cover the Port Townsend region because that elevation data was not updated. Therefore, the Port Townsend mapping of Eungard and others (2018b) is still the most up-to-date.

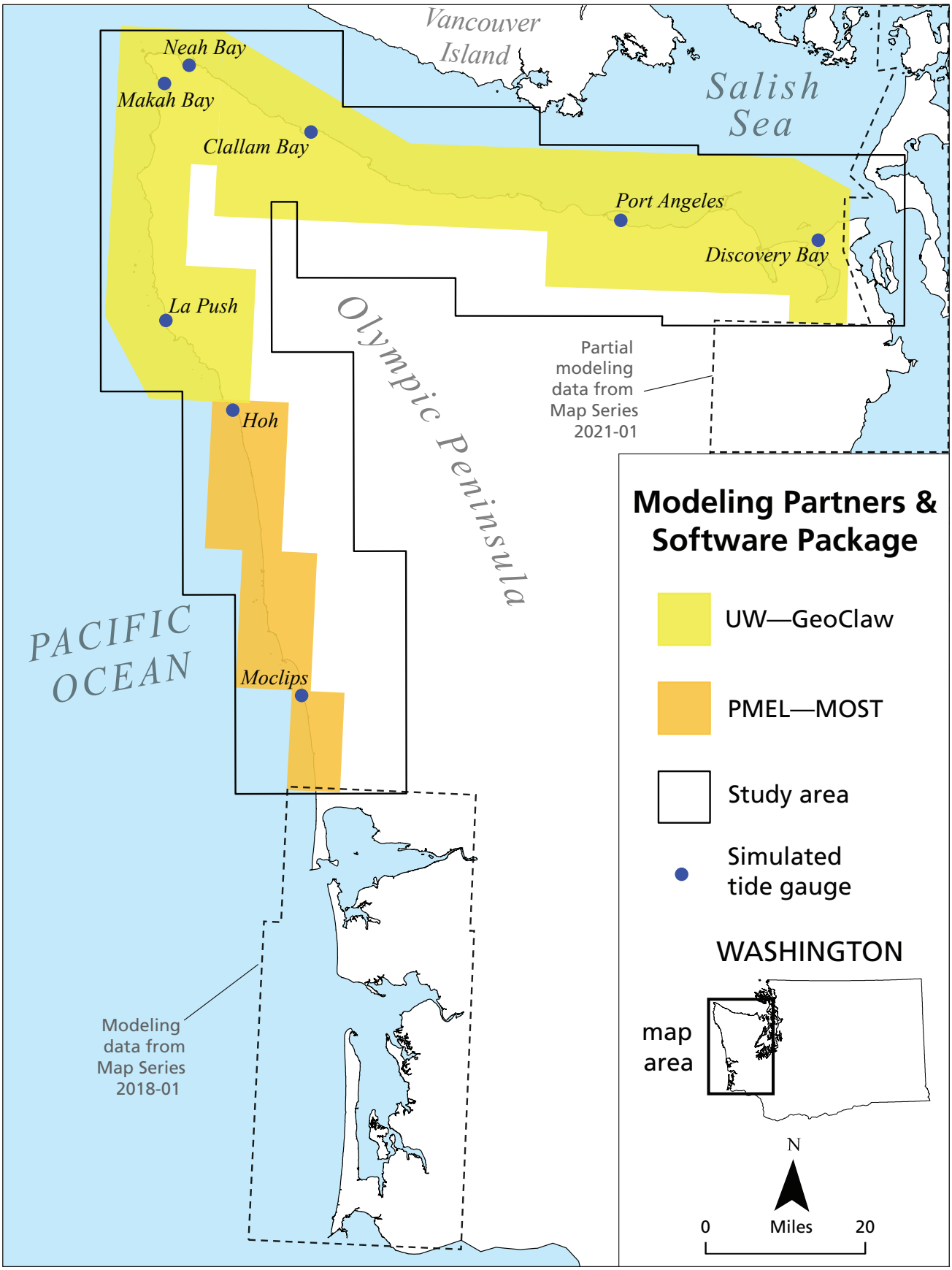

Figure 5. Study areas modeled in this project by the Tsunami Modeling Group at the University of Washington (UW) and the NOAA Center for Tsunami Research at the Pacific Marine Environmental Laboratory (PMEL). For the small region of overlap just north of Hoh, WA, our final model used a compilation of the corresponding model results and prioritized the maximum values. UW used the GeoClaw tsunami modeling software package while PMEL used the Method of Splitting Tsunami (MOST) package. The simulated tide gauges are shown in Figure 7.

The modeling presented in this project also uses high-resolution data from "bare-earth" Digital Elevation Model (DEM) grids, meaning that no forests, built structures, or buildings are included. These elevation grids were provided by NOAA's National Centers for Environmental Information (NOAA National Geophysical Data Center, 2007; 2011; 2015; Cooperative Institute for Research in Environmental Sciences (CIRES) at the University of Colorado, Boulder, 2014). Each grid cell on land within these DEM grids consists of 1/3 arc-second spacing in both the longitude and latitude directions (approximately 23 ft [7 m] and 33 ft [10 m] resolution, respectively).

These tsunami simulations also used either 0.025 or 0.03 for Manning's Roughness Coefficient. These are standard friction values used in tsunami modeling that assume no vegetation and no structures on land, both of which can impede flow or introduce local turbulence, leading our models to produce greater inundation. However, impeded flow could also lead to deeper flow in certain areas with the tsunami wave advancing more slowly inland. Additionally, this assumption may neglect other possible localized effects that vegetation and structures can have on the path and flow of the tsunami. For example, higher fluid velocities may exist in regions where neighboring buildings could channelize flow. This may lead to locally faster current speeds in some heavily built-up urban environments that are not recorded in our model results. A more accurate assessment of tsunami impacts in a built environment would require an additional site-specific study.

RESULTS

The modeling presented here provides tsunami inundation distances, maximum depths, and maximum current speeds using the CSZ Extended L1 scenario for the Olympic Peninsula. Land level change during an earthquake can have a large effect on modeled tsunami impacts. All of the coastal areas included within this study are in close proximity to the subduction zone and the modeled earthquake scenario assumes that their elevations drop (subside) during the earthquake (Fig. 6). This subsidence may cause local flooding prior to tsunami inundation, and a relative rise in sea level compared to pre-earthquake conditions (see below section *Timing of Tsunami Arrival and Initial Water Disturbance*). The modeled earthquake scenario indicates that the most significant drop in land level within this study area occurs at Neah Bay, which subsides approximately 13 ft (4 m). This is a conservative estimate based on our maximum considered earthquake scenario, and is greater than the greatest known paleoseismic subsidence observations recorded on land in Washington (~6 ft or 1.76 m near Cosmopolis, WA, Atwater, 1988; Leonard and others, 2010). Modeled subsidence estimates are smaller in locations east of Port Angeles in the Strait of Juan de Fuca, where subsidence values are 2 ft or less and taper off to a few inches in Discovery Bay. Another location of note is Lake Ozette near the Pacific coast where approximately 6 ft (2 m) of modeled subsidence occurs during the earthquake shaking. This coseismic drop in land and lake level causes disturbances within Lake Ozette, leading to some initial flooding along the eastern lake shoreline prior to the first tsunami wave arrival along the coastline. This is also possible in other lakes on the Olympic Peninsula (such as Lake Crescent) that were not included in the modeled area. Refer to Figure 6 for other locations within the Olympic Peninsula study area with modeled land level change.

Tsunami waves generated from the Extended L1 scenario impact the Pacific coast communities within this study area very soon after the earthquake, leaving limited time for official warnings. Estimated shaking from a large subduction zone earthquake, such as the Extended L1 scenario, could last 3–5 minutes (Megawati and Pan, 2009). This earthquake shaking serves as a warning that a tsunami may be imminent. The first modeled tsunami wave reaches offshore at La Push and Waatch as soon as 10 and 15 minutes, respectively, following the initiation of the earthquake. Other locations along the Pacific Ocean within this study area should expect the first offshore wave arrival within 20 minutes following the beginning of the earthquake shaking. Communities inside the Strait of Juan de Fuca such as Clallam Bay and Port Angeles should expect the first offshore wave arrival at 30 minutes and 1 hour, respectively. The estimated wave arrival times listed throughout this report correspond to the first sign of water levels rising above a reference point. For offshore locations, this is the mean high water (MHW) tidal datum, and for onshore locations is the local ground elevation (Table 2). Map Sheets 1 through 7 depict maximum modeled tsunami inundation and Map Sheets 8 through 14 depict maximum modeled current speed (refer to index map on page iv).

Inundation

Tsunami inundation from the Extended L1 scenario causes extensive flooding along the shorelines of the Olympic Peninsula in northwest Washington. Inundation depths are dependent on surrounding topography, and exceed 60 ft (18 m) along many of the Pacific coastline beaches, campgrounds, and within populated communities throughout this study area (Map Sheets 1–4). Communities that should expect inundation of 60 ft or more include the Hoh Indian Reservation, Queets, Taholah on the Quinault Indian Reservation, Moclips, Pacific Beach, Iron Springs, Copalis Beach, and Ocean City. The greatest amount of inundation occurs near the mouth of the Hoh River and Yellow Banks Beach where flooding depths reach 100 ft (30 m). Other communities along the Pacific coast that experience inundation of 40 ft (6 m) include Waatch on the Makah Indian Reservation, the Ozette Indian Reservation, and La Push, among others. Inundation depths inside the Strait of Juan de Fuca are less severe than on the Pacific coast, though still significant with inundation depths of at least 20 ft (6 m) along the majority of the shoreline (Map Sheets 4–7). Additionally, the tsunami causes some roadways to be impassable, creating intermittent "islands" of land between waves or for many hours until the inundation drains out of the area (we do not model the post-tsunami water drainage). Impassable sections of road occur in some parts of State Route 112 and US Highway 101 south of Discovery Bay. Despite these large depths of flooding, the model results estimate that tsunami inundation is significantly less substantial in the inland and higher elevation areas in proximity to many of these communities (refer to Map Sheets 1–7 for these locations and more detailed inundation values). The Extended L1 scenario also causes significant flooding up rivers and along the tributaries and floodplains of the Quillayute, Dickey, Hoh, Queets, Quinault,

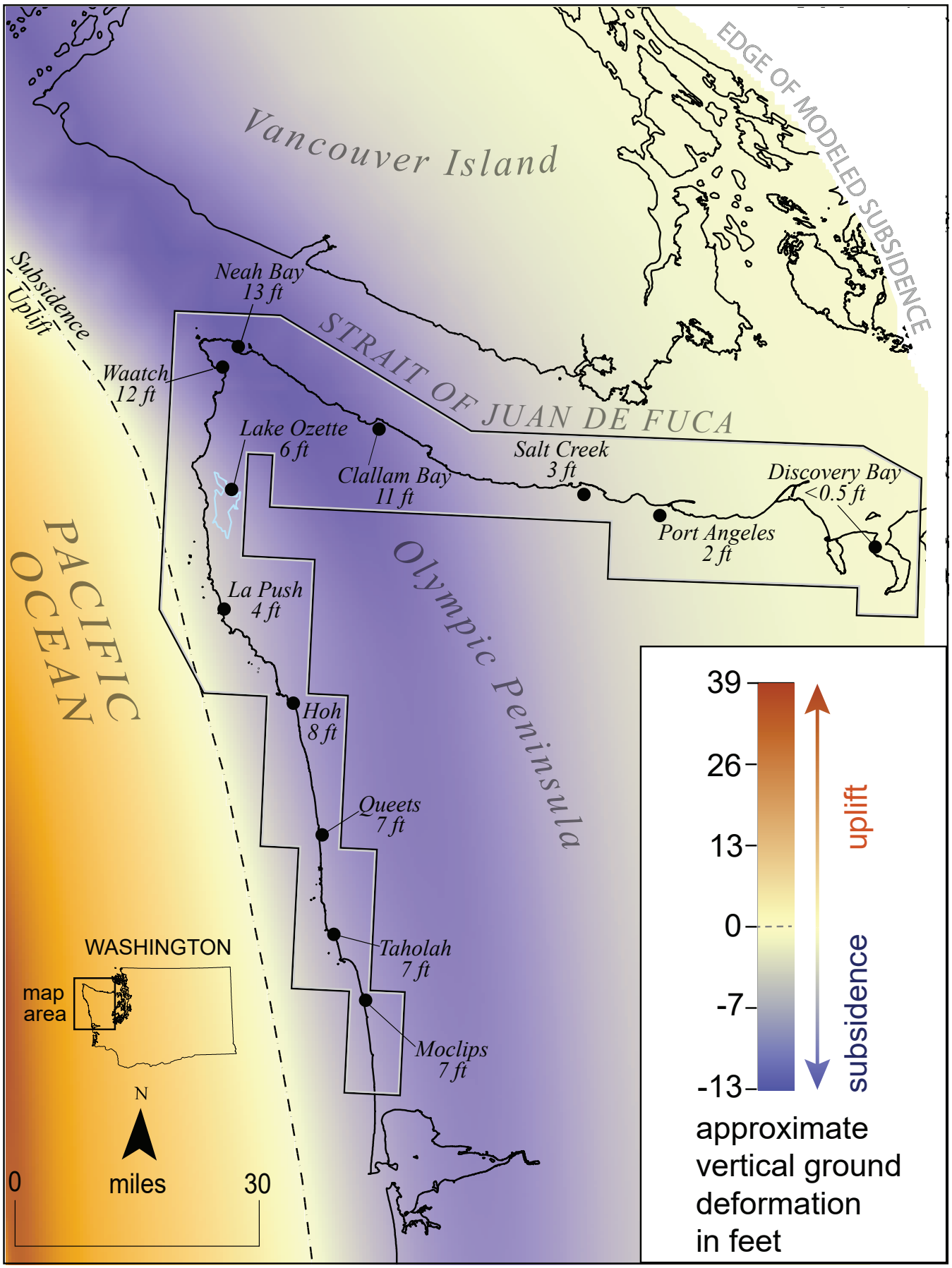

Figure 6. Map of seafloor and land deformation from the Extended L1 scenario. The black polygon outlines the modeled area of the Olympic Peninsula and the black dots represent locations with modeled subsidence values in feet.

Table 2. Tsunami impacts from the CSZ Extended L1 scenario at key locations within the Olympic Peninsula (see "Map sheet number" column on far right of table). Maximum inundation depths and onshore current speeds refer to the entire simulation time. Inundation depth will vary based on local topographic changes. Approximate wave arrivals refer to onshore locations and correspond to the first sign of water levels rising above the local ground elevation reference point. Refer to all map sheets for additional inundation points, current speeds, and wave arrival times.

General location and county	Approximate maximum inundation depth (ft)	Maximum onshore current speed (kn)	Approximate wave arrival (onshore)	Map sheet number
Griffiths-Priday State Park, Grays Harbor	53	9+	20 minutes	1 ,8
Taholah School District, Grays Harbor	43	9+	25 minutes	1, 8
Kalaloch Campground, Jefferson	35	9+	30 minutes	2, 9
Lower Hoh Tribal Center, Jefferson	43	9+	25 minutes	2, 9
Quileute Tribal School, Clallam	31	9+	15 minutes	3, 10
Yellow Banks Beach, Clallam	100	9+	10 minutes	3, 10
Makah Food Bank, Clallam	35	6-9	20 minutes	4, 11
Neah Bay High School, Clallam	20	9+	25 minutes	4, 11
Pillar Point Recreation Area, Clallam	22	6-9	40 minutes	5, 12
Twin Beach, Clallam	19	3-6	45 minutes	5, 12
Lower Elwha Tribal Community, Clallam	9	3-6	1 hour 5 minutes	6, 13
US Coast Guard Air Station Port Angeles, Clallam	15	6-9	1 hour 5 minutes	6, 13
New Dungeness Lighthouse, Clallam	5	3-6	1 hour 20 minutes	7, 14
Highway 20 and US 101 Bus Stop ID: 125, Clallam	33	9+	1 hour 40 minutes	7, 14

Moclips, and Copalis Rivers on the Pacific coast. Tsunami impacts also continue up the Sekiu, Hoko, Pysht, Lyre, Twin, and Elwha Rivers in addition to other creeks in the Strait of Juan de Fuca. In the event of a tsunami, all tributaries and creeks connected to the coast would be intermittently flooded. The modeled study area may not encompass the entirety of all drainage basins, and the extent of flooding from the next tsunami could continue along these river channels and creeks, exceeding the boundaries shown in the modeled map sheets.

Current Speed

The modeled current speed maps (Map Sheets 8–14) show four ranges of water speed in knots (a knot is equal to 1 nautical mile/hr or ~1.15 land mi/hr): 0–3 knots, 3–6 knots, 6–9 knots, and >9 knots. These binned ranges follow the port damage categorization of Lynett and others (2014). The ranges approximate hazard to ships and docking facilities representing: no expected damage (0–3 knots), minor/moderate damage possible (3–6 knots), major damage possible (6–9 knots), and extreme damage possible (>9 knots). Modeled current speeds locally exceed 9 knots, the maximum categorization, along the entire Pacific coastline. Local modeled current speeds exceeding 9 knots are not as widespread in the Strait of Juan de Fuca and mainly occur in Clallam Bay, Port Angeles, Dungeness, Sequim, and the communities along Discovery Bay. Narrower waterway channels and nearshore locations where the tsunami-tide interactions are likely to be most significant should experience the highest speeds but these areas are not explicitly modeled here. Certain topographic features also produce strong currents with potential for the formation of vortices; examples of these features include entrances into harbors and around small islands or land spits with narrow passageways. On Map Sheets 8–14, the regions that show high-speed vortices may be much more widespread than currently shown. This is due to the sensitivity of current speeds in the tsunami modeling—small tweaks in the model setup cause these vortices to take slightly different paths. As a result, the spatial extents of these vortices are only estimates.

Timing of Tsunami Arrival and Initial Water Disturbance

Estimated wave arrival times for a given location correspond to the time elapsed from the beginning of earthquake shaking to when water first rises above a reference point (MHW tidal datum for offshore and local ground elevation for onshore). This timing may also reflect localized flooding from subsidence prior to the first tsunami-generated wave for shoreline locations (as discussed

with Lake Ozette), and does not account for falling water levels that precede the first incoming rising wave for offshore locations. For example, an estimated offshore wave arrival of 15 minutes means the first rising wave above MHW would arrive at that location 15 minutes after the earthquake begins. However, in a real event, the actual flooding onset also depends on the tide stage when the wave impinges on the shoreline. The arrival times shown on all map sheets are the arrival times of the first wave, which may not necessarily be the largest wave. Several minutes or even hours may pass between first wave arrival and another wave that brings maximum current speed, inundation depth, or inundation extent. Strong earthquake shaking may persist for as much as 5 minutes in this scenario, reducing the available time to evacuate. In the event of a large Cascadia earthquake, the tsunami wave initiates at the uplift of a splay fault and then travels to the Pacific coast and into the Strait of Juan de Fuca very rapidly. Figure 7 shows a series of simulated synthetic tide gauge records for selected locations along the Pacific coast and within the Strait of Juan de Fuca. In this study area, the first modeled wave arrives at La Push within approximately 10 minutes (Fig. 7B).

Simulated tide gauges estimate the approximate timing of the initial water disturbance. A tsunami either arrives as a trough (pulling water out and away from shore) or a crest (rapidly rising flood of water toward shore). This is a function of distance and position to the subduction zone. Tsunamis with leading troughs generally cause larger flooding depths than tsunamis with leading crests (Tadepalli and Synolakis, 1994). In the case of the CSZ, an initial trough occurs along Washington's shorelines prior to a wave crest.

For all locations in this study area, the Extended L1 scenario earthquake model instantaneously deforms the ocean and land topography relative to pre-earthquake conditions, creating both coseismic subsidence and coseismic uplift. Along the Pacific coast, an initial drop in elevation due to earthquake subsidence leads to rapid, localized flooding of low-lying areas within minutes of the earthquake (Fig 8). When local land and sea levels drop during the earthquake, global sea level does not, so water rushes back inland to correct the sudden imbalance. Due to this localized flooding, the leading trough of the tsunami may not be noticeable prior to the rising wave that arrives along the Pacific coast within 10–20 minutes of the start of the earthquake. The rising wave continues to increase in amplitude, reaching crests in excess of ~30 ft (9 m), though locally approaching 70 ft along the Pacific coast and nearly 20 ft (6 m) at Neah Bay within approximately 30 and 40 minutes, respectively (Fig. 7).

Tsunami waves in locations farther into the Strait of Juan de Fuca would arrive later. Later wave arrival times allow for more noticeable troughs to occur before the first rising wave. However, leading troughs would still follow any initial localized flooding due to subsidence associated with the earthquake. Locations inside the Strait of Juan de Fuca are close enough to the subduction zone to experience coseismic subsidence, but are far enough away for the local sea level to marginally recover before the leading trough of the tsunami arrives. For example, at Port Angeles the land and water levels suddenly drop ~2 ft during the shaking of the earthquake, rise slightly in an effort to recreate a balance between local and global sea levels, and then draw out approximately 15 minutes later with the arrival of the tsunami trough (Fig 7G; Fig 8). After the initial trough in Port Angeles, the modeled wave begins to rise above MHW around 1 hour after the start of the earthquake. An ~20 ft wave crest then follows 30 minutes later.

DISCUSSION

Hypothetically, if the next CSZ earthquake is only a partial rupture and does not occur directly offshore Washington (not the Extended L1 scenario), coseismic subsidence could be minimal and rapid, and local flooding may be absent in some locations prior to the first tsunami wave. Due to the orientation of the CSZ relative to the Olympic Peninsula, a southern partial-rupture with negligible subsidence along Washington's coast could cause the first tsunami wave to have a more appreciable trough prior to the first rising wave arrival. This phenomenon of water receding from the shore provides visual evidence, in addition to shaking, that a tsunami is approaching.

At inundation depths greater than 6 feet, survival is unlikely for persons out in the open or within or on most conventional structures. Fortunately, survival remains highly likely within or on a reinforced and specially designed building, such as a vertical evacuation structure. For places where inundation depths are less than 6 feet, survivability is still unlikely for persons caught in the open. However, chances can be improved if proper steps are taken to avoid the direct force of a wave. For example, if high ground is unreachable, entering an upper story of a sturdy building, climbing onto the roof of a sturdy building, or climbing a strong tree could be an effective last resort (Atwater and others, 1999). These measures can greatly increase survivability if the wave is less than head-high. For waves that are less than knee-high, and if high ground is unavailable, standing on the leeward side of an obstacle (tree or power pole) could also be an effective last resort to avoid direct impact of objects that are carried in the water, which may cause significant injury. Lastly, if swept up by a tsunami, climbing onto something that floats could serve as a life raft (Atwater and others, 1999).

Modeled wave crests larger than 10 ft continue to bombard all of the Olympic Peninsula's shorelines within this study until about 4 hours after the earthquake. We anticipate that significant wave activity could also continue for 8 or more hours following the earthquake based on historical events. Minor inundation and strong currents may pose a hazard to rescue and recovery operations and may continue for 24 or more hours after the earthquake. For comparison, the March 27, 1964 Mw 9.2 earthquake near Anchorage, Alaska affected local wave currents offshore Alaska for days. That event also produced its most noticeable wave in Washington (near Raymond and South Bend in Willapa Bay) about 12 hours after the first wave reached Washington's Pacific coast (Walsh and others, 2000). In addition, the January 26, 1700 earthquake along the CSZ produced a tsunami that may have lasted as many as 20 hours in Japan (Satake and others, 2003; Atwater and others, 2005).

LIMITATIONS OF THE MODEL

The rupture patterns of earthquakes on a given subduction zone often vary significantly from one earthquake sequence to the

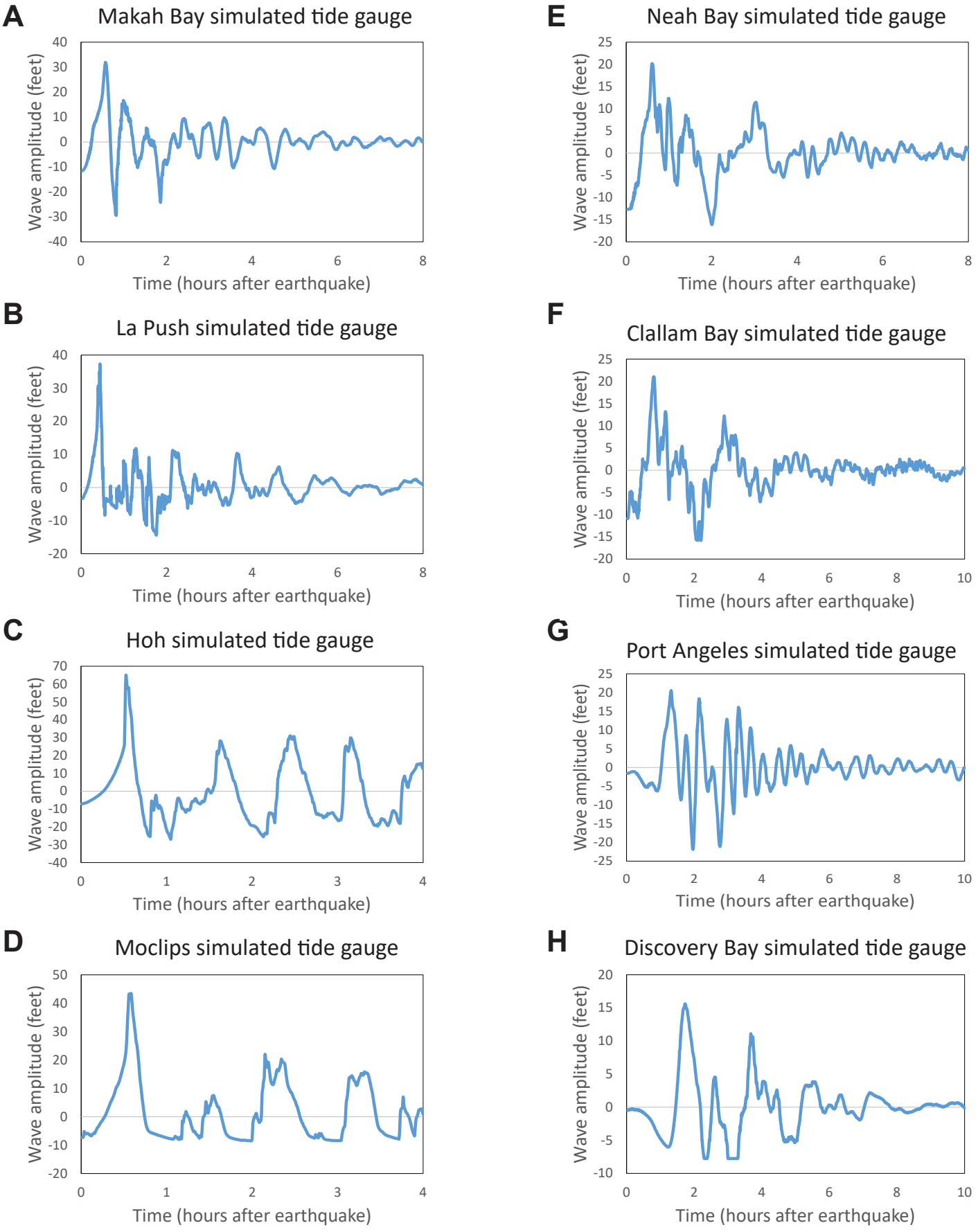

Figure 7. Modeled tsunami wave variations over time (light blue lines) for eight simulated tide gauges in **A.** Makah Bay, **B.** La Push (East of James Island), **C.** Hoh, **D.** Moclips, **E.** Neah Bay, **F.** Clallam Bay, **G.** Port Angeles, and **H.** Discovery Bay. Subfigures A–D are for the Pacific Coast and subfigures E–H are for the Strait of Juan de Fuca.Gray horizontal lines indicate static mean high water elevation at simulated tide gauges. Refer to Fig. 5 and Map Sheets 1–7, respectively for locations.

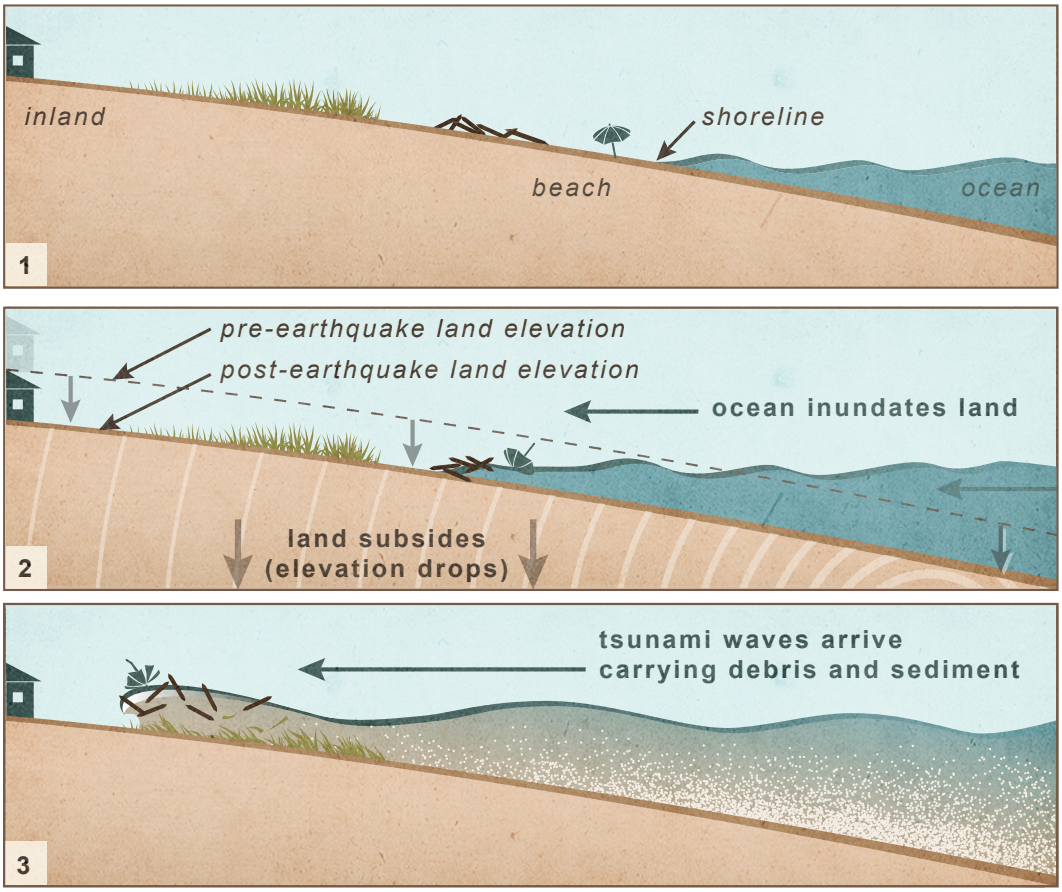

Figure 8. Schematic diagram of chronologic events following a CSZ earthquake and tsunami for the Pacific coast. (1) Modern-day pre-earthquake topography. (2) Large earthquake on the CSZ produces strong shaking that may last several minutes. During the earthquake event, the land and local sea level subsides or "drops", causing local flooding of low-lying areas within minutes of the earthquake. Note that within the Strait of Juan de Fuca, a leading wave trough of the tsunami still occurs following any local flooding prior to arrival of the first tsunami wave crest. Submarine landslides triggered by seismic shaking are also possible, which could result in locally generated tsunamis with leading rising waves. (3) Tsunami waves begin to arrive. These powerful waves carry sediment and debris onshore and to higher elevations. The wave inundation may continue for at least 8 hours locally, posing a hazard to search, rescue, and recovery efforts. Once tsunami inundation floodwaters recede, a new shoreline is established many feet higher in elevation than before.

next. In addition, because there have been no direct observations of previous coseismic slip produced in a large CSZ earthquake, researchers do not have a strong understanding of the resultant pattern of seafloor deformation. The Extended L1 scenario used in this study is deterministic and has a simplified regional slip distribution that only takes into account the static, vertical component of seafloor displacement for tsunami generation (Witter and others, 2011). This scenario ruptures instantaneously in our modeling along the CSZ margin, and does not include other potential components that could alter the tsunami generation (such as material heterogeneity in the subduction zone, inelastic behavior, horizontal slip components, extensional faults within the subduction zone, or dynamic coseismic deformation). The largest source of uncertainty in this modeling is therefore the input earthquake deformation. The earthquake scenario used in this model consists of a surface-rupturing splay fault that was estimated to approximate the 2 percent probability of exceedance in 50 years, but the next earthquake may have a more complex slip distribution and rupturing geometry than the modeled scenario. For example, other megathrust earthquake scenarios that do not rupture an active splay fault (which in turn have their own uncertainty)(Wang and Tréhu, 2016) or that have along-strike heterogeneity (see M9 project: https://hazards.uw.edu/geology/m9/) are possible too.

The tsunami modeling packages do not include the influences of changes in tides or projected sea-level rise. The tide stage can amplify or reduce the impact of a tsunami on a specific community. For example, the diurnal range (the difference in height between mean higher high water and mean lower low water) is 7.96 ft (2.43 m), 8.52 ft (2.60 m), and 7.06 ft (2.15 m) at the Neah Bay, La Push, and Port Angeles tide gauge stations in Clallam County, respectively (NOAA, 2021a,b,c). The model does not include riverine flow nor interaction with tidal currents. Tidal currents can be additive if in the same direction or steepen the tsunami wave front and cause a breaking wave if in an opposing direction (Zhang and others, 2011). The model also does not include interactions between an ebbing wave and a subsequent flooding wave.

The bathymetry and topography data used to make the elevation grid limits the resolution of the modeling. A variety of data sources contributed to the elevation grid, with grid cells of ~3 ft (1 m) for the topographic grid and ~16–3,937 ft (5–1,200 m) for the bathymetric grid. Coarse grids do not capture small topographic features that can influence the tsunami locally. Coarse grids generally lead to greater modeled inundation than would be produced by finer grids, except in narrow or constricted channels or along steep topographic features.

These model results do not account for the possibility of seismically induced seiches or landslides resulting from the earthquake. Seiches are a series of standing waves that may occur in fully or partially enclosed bodies of water, such as Lake Ozette, when earthquake waves pass through. This could lead to greater flooding along lake shorelines than shown in the model results. These results also do not include potential tsunamis from coseismic landslides, which may be triggered by a CSZ earthquake. Additionally, the modeling does not include any foreshocks or aftershocks, which may also cause slope failures that could generate tsunamis in inland waters (including lakes).

Local slope failures have the potential to generate tsunamis that arrive even earlier than the times estimated within this publication. This modeling does not incorporate localized topographic changes caused by sediment erosion or liquefaction, such as settlement or sand blows. All of these effects are beyond the scope of this study.

CONCLUSION

The new modeling presented here provides estimates of tsunami inundation distance, maximum inundation depths, maximum current speeds, and first wave arrival times for the Olympic Peninsula. The Extended L1 scenario is estimated to encompass 95 percent of the variability in tsunami sources, and produces a tsunami that is unlikely, though not impossible, to be exceeded. Modeling results show that certain locations would experience inundation depths in excess of 60 feet (18 m) along the Pacific coast and 20 feet (6 m) within the Strait of Juan de Fuca. Many waterways would experience current speeds in excess of 9 knots throughout the entirety of the study area. The first tsunami waves generated from the earthquake would reach La Push on the Pacific coast within approximately 10 minutes and Neah Bay at the entrance of the Strait of Juan de Fuca within about 20 minutes, though local flooding from coseismic subsidence prior to the first tsunami wave arrival could occur within minutes after the start of the earthquake. Additionally, any coseismic subsidence will establish a new shoreline once the earthquake is over.

Despite some limitations to our model, meaning that the model does not provide an exact representation of a tsunami generated by an earthquake on the Cascadia subduction zone, the results presented here are valuable for regional awareness and hazard planning. We emphasize that planning for tsunami hazards also includes planning for earthquake hazards. We hope this information will be used to increase community resilience to tsunamis and earthquakes in the Olympic Peninsula.

ACKNOWLEDGMENTS

The National Tsunami Hazard Mitigation Program (NTHMP) in cooperation with cities, counties, tribes, and the Washington Emergency Management Division supported this project. The NTHMP aims to reduce the impact of tsunamis through warning guidance, hazard assessment, and mitigation. This project was partially funded by NOAA Award NA20NWS4670068. This does not constitute an endorsement by NOAA. This is PMEL contribution 5329. We acknowledge the work of the WGS publications team for their effort in producing the map sheets, specifically Daniel Coe and Maria Furtney. We also would like to acknowledge the computing time provided by the CU-CSDMS High-Performance Computing Cluster, and by the Applied Mathematics Department at the University of Washington. This work would also not be possible without the seminal work done regarding the Cascadia subduction zone earthquake source model by Witter and others (2011).

REFERENCES

Adams, John, 1990, Paleoseismicity of the Cascadia subduction zone: Evidence from turbidites off the Oregon–Washington margin: Tectonics, v. 9, no. 4, p. 569–583. [https://doi.org/10.1029/TC009i004p00569]

Atwater, B. F., 1992, Geologic evidence for earthquakes during the past 2000 years along the Copalis River, southern coastal Washington: Journal of Geophysical Research, v. 97, no. B2, p. 1901–1919. [https://doi.org/10.1029/91JB02346]

Atwater, B. F., 1988, Geologic studies for seismic zonation of the Puget Lowland. *In* Jacobson, M. L.; Rodriguez, T. R., compilers, National Earthquake Hazards Reduction Program, Summaries of technical reports, Volume XXV: U.S. Geological Survey Open-File Report 88–16, p. 120–133. [https://doi.org/10.3133/ofr8816]

Atwater, B. F.; Vega, M. C.; Bourgeois, Joanne; Dudley, W. C.; Hendley, J. W., II; Stauffer, P. H., 1999, Surviving a tsunami—Lessons from Chile, Hawaii, and Japan: U.S. Geological Survey Circular 1187, v. 1, 19 p. [https://pubs.usgs.gov/circ/c1187/]

Atwater, B. F.; Carson, Bobb; Griggs, G. B.; Johnson, H. P.; Salmi, M. S., 2014, Rethinking turbidite paleoseismology along the Cascadia subduction zone: Geology, v. 42, no. 9, p. 827–830. [https://doi.org/10.1130/G35902.1]

Atwater, B. F.; Hemphill-Haley, Eileen, 1997, Recurrence intervals for great earthquakes of the past 3,500 years at northeastern Willapa Bay, Washington: U.S. Geological Survey Professional Paper 1576, 108 p. [https://doi.org/10.3133/pp1576]

Atwater, B. F.; Nelson, A. R.; Clague, J. J.; Carver, G. A.; Yamaguchi, D. K.; Bobrowsky, P. T.; Bourgeois, Joanne; Darienzo, M. E.; Grant, W. C.; Hemphill-Haley, Eileen; Kelsey, H. M.; Jacoby, G. C.; Nishenko, S. P.; Palmer, S. P.; Peterson, C. D.; Reinhart, M. A., 1995, Summary of coastal geologic evidence for past great earthquakes at the Cascadia subduction zone: Earthquake Spectra, v. 11, no. 1, 18 p. [https://doi.org/10.1193/1.1585800]

Atwater, B. F.; Satoko, Musumi-Rokkaku; Kenji, Satake; Yoshinobu, Tsuji; Kazue, Ueda; Yamaguchi, D. K., 2005, The orphan tsunami of 1700—Japanese clues to a parent earthquake in North America: U.S. Geological Survey in association with University of Washington Press, U.S. Geological Survey Professional Paper 1707, 135 p. [https://doi.org/10.3133/pp1707]

Atwater, B. F.; Yamaguchi, D. K., 1991, Sudden, probably coseismic submergence of Holocene trees and grass in coastal Washington State: Geology, v. 19, no.7, p. 706–709. [https://doi.org/10.1130/0091-7613(1991)019<0706:SPCSOH>2.3.CO;2]

Berger, M. J.; George, D. L.; LeVeque, R. J.; Mandli, K. T., 2011, The GeoClaw software for depth-averaged flows with adaptive refinement: Advances in Water Resources, v. 34, no. 9, p. 1195–1206. [https://doi.org/10.1016/j.advwatres.2011.02.016]

Clawpack Development Team, 2021, Clawpack Versions 5.7.0–5.8.0, http://www.clawpack.org. [https://doi.org/10.17605/osf.io/kmw6h]

Cooperative Institute for Research in Environmental Sciences (CIRES) at the University of Colorado, Boulder, 2014, Continuously Updated Digital Elevation Model (CUDEM)–1/9 Arc-second resolution bathymetric-topographic tiles for the Outer Coast and Strait of Juan de Fuca: NOAA National Centers for Environmental Information, prepublication version provided by NCEI in 2020. [https://doi.org/10.25921/ds9v-ky35]

Dolcimascolo, Alexander; Eungard, D. W.; Allen, Corina; LeVeque, R. J.; Adams, L. M.; Arcas, Diego; Titov, V. V.; González, F. I.; Moore, Christopher; Garrison-Laney, C. E.; Walsh, T. J., 2021, Tsunami hazard maps of the Puget Sound and adjacent waters—Model results from an extended L1 Mw 9.0 Cascadia subduction zone megathrust earthquake scenario: Washington Geological Survey Map Series 2021-01, 16 sheets, scale 1:48,000, 49 p. text. [https://fortress.wa.gov/dnr/geologydata/tsunami_hazard_maps/ger_ms2021-01_tsunami_hazard_puget_sound.zip]

Eungard, D. W.; Forson, Corina; Walsh, T. J.; Gica, Edison; Arcas, Diego, 2018a, Tsunami hazard maps of the Anacortes–Bellingham area, Washington—Model results from a ~2,500-year Cascadia subduction zone earthquake scenario: Washington Geological Survey Map Series 2018-02, 6 sheets, scale 1:30,000, 10 p. text. [https://www.dnr.wa.gov/publications/ger_ms2018-02_tsunami_hazard_anacortes_bellingham.zip]

Eungard, D. W.; Forson, Corina; Walsh, T. J.; González, F. I.; LeVeque, R. J; Adams, L. M., 2018b, Tsunami hazard maps of Port Angeles and Port Townsend, Washington—Model results from a ~2,500-year Cascadia subduction zone earthquake scenario: Washington Geological Survey Map Series 2018-03, 6 sheets, scale 1:11,000 and 1:16,000, 11 p. text. [http://www.dnr.wa.gov/publications/ger_ms201803_tsunami_hazard_pt_angeles_pt_townsend.zip]

Eungard, D. W.; Forson, Corina; Walsh, T. J.; Gica, Edison; Arcas, Diego, 2018c, Tsunami hazard maps of southwest Washington—Model results from a ~2,500-year Cascadia subduction zone earthquake scenario: Washington Geological Survey Map Series 2018-01, originally published March 2018, 6 sheets, scale 1:48,000, 11 p. text. [http://www.dnr.wa.gov/publications/ger_ms201801_tsunami_hazard_southwest_washington.zip]

Flück, Paul; Hyndman, R. D.; Wang, Kelin, 1997, Three-dimensional dislocation model for great earthquakes of the Cascadia Subduction Zone: Journal of Geophysical Research: Solid Earth, v. 102, no. B9, p. 20539–20550. [https://doi.org/10.1029/97JB01642]

Garrison-Laney, C. E., 2017, Tsunamis and sea levels of the past millennium in Puget Sound, Washington: University of Washington Doctor of Philosophy thesis, 166 p. [https://digital.lib.washington.edu/researchworks/handle/1773/40393]

Garrison-Laney, C. E.; Miller, Ian, 2017, Tsunamis in the Salish Sea: Recurrence, sources, hazards. *In* Haugerud, R. A.; Kelsey, H. M., editors, 2017, From the Puget Lowland to east of the Cascade Range: Geologic excursions in the Pacific Northwest: Geological Society of America Field Guide 49, p. 67–78. [https://doi.org/10.1130/2017.0049(04)]

George, D. L., 2008, Augmented Riemann solvers for the shallow water equations over variable topography with steady states and inundation: Journal of Computational Physics, v. 227, no. 6, p. 3089–3113. [https://doi.org/10.1016/j.jcp.2007.10.027]

George, D. L., 2006, Finite volume methods and adaptive refinement for tsunami propagation and inundation: University of Washington Doctor of Philosophy thesis, 167 p. [https://digital.lib.washington.edu/researchworks/handle/1773/4639]

George, D. L.; LeVeque, R. J., 2006, Finite volume methods and adaptive refinement for global tsunami propagation and local inundation: Science of Tsunami Hazards, v. 24, no. 5, p. 319–328. [https://digital.lib.washington.edu/researchworks/bitstream/handle/1773/4639/tsunami06.pdf]

Gica, Edison; Arcas, Diego, 2015, Tsunami inundation modeling of Seattle and Tacoma due to a Cascadia subduction zone earthquake: National Oceanic and Atmospheric Administration Center for Tsunami Research, unpublished report, 44 p.

Griggs, G. B., 1968, Cascadia Channel: The anatomy of a deep-sea channel: Oregon State University Doctor of Philosophy thesis, 185 p. [https://ir.library.oregonstate.edu/concern/graduate_thesis_or_dissertations/j96022953]

Griggs, G. B.; Kulm, L. D., 1970, Sedimentation in Cascadia deep-sea channel: Geological Society of America Bulletin, v. 81, no. 5, p. 1361–1384. [https://doi.org/10.1130/0016-7606(1970)81[1361:SICDC]2.0.CO;2]

Goldfinger, Chris; Galer, Steve; Beeson, Jeffrey; Hamilton, Tark; Black, Bran; Romsos, Chris; Patton, Jason; Nelson, C. H.; Hausmann, Rachel; Morey, Ann, 2017, The importance of site selection, sediment supply, and hydrodynamics: A case study of submarine paleoseismology on the northern Cascadia margin, Washington, USA: Marine Geology, v. 384, no. 17, p 25–46. [https://doi.org/10.1016/j.margeo.2016.06.008]

Goldfinger, Chris; Morey, A. E.; Black, Bran; Beeson, Jeffrey; Nelson, C. H.; Patton, Jason, 2013, Spatially limited mud turbidites on the Cascadia margin: Segmented earthquake ruptures?: Natural Hazards and Earth System Sciences, v. 13, no. 8, p. 2109–2146. [https://doi.org/10.5194/nhess-13-2109-2013]

Goldfinger, Chris; Nelson, C. H.; Morey, A. E.; Johnson, J. E.; Patton, J. R.; Karabanov, E. B.; Gutierrez-Pastor, Julia; Eriksson, A. T.; Gracia, Eulalia; Dunhill, Gita; Enkin, R. J.; Dallimore, Audrey; Vallier, Tracy, 2012, Turbidite event history—Methods and implications for Holocene paleoseismicity of the Cascadia Subduction Zone: U.S. Geological Survey Professional Paper 1661-F, 170 p. [https://doi.org/10.3133/pp1661F]

González, F. I.; LeVeque, R. J.; Chamberlain, Paul; Hirai, Bryant; Varkovitsky, Jonathan; George, D. L., 2011, Validation of the GeoClaw model—NTHMP MMS tsunami inundation model validation workshop: University of Washington, 84 p. [https://depts.washington.edu/clawpack/links/nthmp-benchmarks/geoclaw-results.pdf]

Heaton, T. H.; Snavely, P. D., Jr., 1985, Possible tsunami along the northwestern coast of the United States inferred from Indian traditions: Bulletin of the Seismological Society of America, v. 75, no. 5, p. 1455–1460. [https://doi.org/10.1785/BSSA0750051455]

Henderson, Bonnie, 2014, The next tsunami: Living on a restless coast: Oregon State University Press, 330 p. [https://osupress.oregonstate.edu/book/next-tsunami]

Horrillo, Juan; Grilli, S. T.; Nicolsky, Dmitry; Roeber, Volker; Zhang, Joseph, 2015, Performance benchmarking tsunami models for NTHMP's inundation mapping activities: Pure and Applied Geophysics, v. 172, no. 3–4, p. 869–884. [https://doi.org/10.1007/s00024-014-0891-y]

Hutchinson, Ian; Clague, John, 2017, Were they all giants? Perspectives on late Holocene plate-boundary earthquakes at the northern end of the Cascadia subduction zone: Quaternary Science Reviews, v. 169, p. 29–49. [https://doi.org/10.1016/j.quascirev.2017.05.015]

Hutchinson, Ian; Peterson, C. D.; Sterling, S. L., 2013, Late Holocene tsunami deposits at Salt Creek, Washington, USA: Science of Tsunami Hazards, v. 32, p. 221–235. [http://archives.pdx.edu/ds/psu/12419]

International Code Council, 2015, 2015 International Building Code, 690 p. [https://codes.iccsafe.org/content/IBC2015]

Jacoby, G. C.; Bunker, D. E.; Benson, B. E., 1997, Tree-ring evidence for an A.D. 1700 Cascadia earthquake in Washington and northern Oregon: Geology, v. 25, no. 11, p. 999–1002. [https://doi.org/10.1130/0091-7613(1997)025<0999:TREFAA>2.3.CO;2]

Kelsey, H. M.; Nelson, A. R.; Hemphill-Haley, Eileen; Witter, R. C., 2005, Tsunami history of an Oregon coastal lake reveals a 4600 yr record of great earthquakes on the Cascadia subduction zone: Geological Society of America Bulletin, v. 117, no. 7–8, p. 1009–1032. [https://doi.org/10.1130/B25452.1]

Kelsey, H. M.; Witter, R. C.; Hemphill-Haley, Eileen, 2002, Plate-boundary earthquakes and tsunamis of the past 5500 yr, Sixes River estuary, southern Oregon: Geological Society of America Bulletin, v. 114, no. 3, p. 298–314. [https://doi.org/10.1130/0016-7606(2002)114<0298:PBEATO>2.0.CO;2]

Leonard, L. J.; Currie, C. A.; Mazzotti, Stéphane; Hyndman, R. D., 2010, Rupture area and displacement of past Cascadia great earthquakes from coastal coseismic subsidence: Geological Society of America Bulletin, v. 122, no. 11–12, p. 2079–2096. [https://doi.org/10.1130/B30108.1]

LeVeque, R. J.; George, D. L.; Berger, M. J, 2011, Tsunami modelling with adaptively refined finite volume methods: Acta Numerica, v. 20, p. 211–289. [https://doi.org/10.1017/S0962492911000043]

Ludwin, R. S., 2002, Cascadia megathrust earthquakes in Pacific Northwest Indian myths and legends: TsuInfo Alert, v. 4, no. 2, p. 6–10. [https://www.dnr.wa.gov/publications/ger_tsuinfo_2002_v4_no2.pdf]

Lynett, P. J.; Borrero, Jose; Son, Sangyoung; Wilson, Rick; Miller, Kevin, 2014, Assessment of the tsunami-induced current hazard: Geophysical Research Letters, v. 41, no. 6, p. 2048–2055. [https://doi.org/10.1002/2013GL058680]

Mandli, K. T.; Ahmadia, A. J.; Berger, Marsha; Calhoun, Donna; George, D. L.; Hadjimichael, Yiannis; Ketcheson, D. I.; Lemoine, G. I.; LeVeque, R. J., 2016, Clawpack: Building an open source ecosystem for solving hyperbolic PDEs: PeerJ Computer Science, v. 2, no. e68, 27 p. [https://doi.org/10.7717/peerj-cs.68]

Megawati, Kusnowidjaja; Pan, Tso-Chien, 2009, Regional seismic hazard posed by the Mentawi segment of the Sumatran megathrust: Bulletin of the Seismological Society of America, v. 99, no. 2A, p. 566–584. [https://doi.org/10.1785/0120080109]

Morton, R. A.; Gelfenbaum, Guy; Jaffe, B. E., 2007, Physical criteria for distinguishing sandy tsunami and storm deposits using modern examples: Sedimentary Geology, v. 200, no. 3–4, p. 184–207. [https://doi.org/10.1016/j.sedgeo.2007.01.003]

Myers, E. P.; Baptista, A. M.; Priest, G. R., 1999, Finite element modeling of potential Cascadia subduction zone tsunamis: Science of Tsunami Hazards, v. 17, no. 1, p. 3–18. [https://library.lanl.gov/tsunami/ts171.pdf]

National Oceanic and Atmospheric Administration, 2021a, Datums for 9442396, La Push, Quillayute River WA [webpage]: National Oceanic and Atmospheric Administration. [accessed Aug. 23, 2021 at https://tidesandcurrents.noaa.gov/datums.html?id=9442396]

National Oceanic and Atmospheric Administration, 2021b, Datums for 9443090, Neah Bay WA [webpage]: National Oceanic and Atmospheric Administration. [accessed Aug. 23, 2021 at https://tidesandcurrents.noaa.gov/datums.html?id=9443090]

National Oceanic and Atmospheric Administration, 2021c, Datums for 9444090, Port Angeles WA [webpage]: National Oceanic and Atmospheric Administration. [accessed Aug. 23, 2021 at https://tidesandcurrents.noaa.gov/datums.html?id=9444090]

Nelson, A. R.; Kelsey, H. M.; Witter, R. C., 2006, Great earthquakes of variable magnitude at the Cascadia subduction zone: Quaternary Research, v. 65, no. 3, p. 354–365. [https://doi.org/10.1016/j.yqres.2006.02.009]

NOAA National Geophysical Data Center, 2011, Port Townsend, Washington 1/3 Arc-second MHW Coastal Digital Elevation Model: NOAA National Centers for Environmental Information. [accessed May 2021 at https://www.ncei.noaa.gov/metadata/geoportal/rest/metadata/item/gov.noaa.ngdc.mgg.dem:366/html]

NOAA National Geophysical Data Center, 2015, Strait of Juan de Fuca 1/3 arc-second NAVD 88 Coastal Digital Elevation Model: NOAA National Centers for Environmental Information. [accessed May 2021 at https://www.ncei.noaa.gov/metadata/geoportal/rest/metadata/item/gov.noaa.ngdc.mgg.dem:11514/html].

NOAA National Geophysical Data Center, 2007, La Push, Washington 1/3 arc-second MHW Coastal Digital Elevation Model: NOAA National Centers for Environmental Information. [accessed August 2020 at https://data.noaa.gov/metaview/page?xml=NOAA/NESDIS/NGDC/MGG/DEM//iso/xml/247.xml&view=getDataView&header=none#]

Padgett, J. S.; Engelhart, S. E.; Kelsey, H. M.; Witter, R. C.; Cahill, Niamh; Hemphill-Haley, Eileen, 2021, Timing and amount of southern Cascadia earthquake subsidence over the past 1700 years at northern Humboldt Bay, California, USA: Geological Society of America Bulletin, v. 133, no. 9–10, p. 2137–2156. [https://doi.org/10.1130/B35701.1]

Peters, Robert; Jaffe, B. E.; Gelfenbaum, Guy; Peterson, Curt, 2003, Cascadia tsunami deposit database: U.S. Geological Survey Open-File Report 2003-13, 25 p. [https://doi.org/10.3133/ofr0313]

Petersen, M. D.; Moschetti, M. P.; Powers, P. M.; Mueller, C. S.; Haller, K. M.; Frankel, A. D.; Zeng, Yuehua; Rezaeian, Sanaz; Harmsen, S. C.; Boyd, O. S.; Field, E. H.; Chen, Rui; Rukstales, K. S.; Luco, Nico; Wheeler, R. L.; Williams, R. A.; Olsen, A. H., 2014, Documentation for the 2014 update of the United States national seismic hazard maps: U. S. Geological Survey Open-File Report 2014–1091, 243 p. [https://doi.org/10.3133/ofr20141091]

Peterson, C. D.; Cruikshank, K. M.; Darienzo, M. E.; Wessen, G.C.; Butler, V. L.; Sterling, S. L., 2013, Coseismic subsidence and paleotsunami run-up records from latest Holocene deposits in the Waatch Valley, Neah Bay, northwest Washington, U.S.A.: Links to great earthquakes in the northern Cascadia margin: Journal of Coastal Research, v. 29, no. 1, p. 157–172. [https://doi.org/10.2112/JCOASTRES-D-12-00031.1]

Plafker, George, 1969, Tectonics of the March 27, 1964 Alaska earthquake: U.S. Geological Survey Professional Paper 543-I, 74 p., 2 sheets, scales 1:2,000,000 and 1:500,000. [https://pubs.usgs.gov/pp/0543i/].

Plafker, George; Savage, J. C., 1970, Mechanism of the Chilean earthquakes of May 21 and 22, 1960: Geological Society of America Bulletin, v. 81, no. 4, p. 1001–1030. [https://doi.org/10.1130/0016-7606(1970)81[1001:MOTCEO]2.0.CO;2]

Priest, G. R.; Myers, E. P., III; Baptista, A. M.; Fleuck, Paul; Wang, Kelin; Kamphaus, R. A.; Peterson, C. D., 1997, Cascadia subduction zone tsunamis: Hazard mapping at Yaquina Bay, Oregon: Oregon Department of Geology and Mineral Industries Open-File Report O-97-34, 144 p. [http://www.oregongeology.org/pubs/ofr/O-97-34.pdf]

Priest, G. R.; Zhang, Yinglong; Witter, R. C.; Wang, Kelin; Goldfinger, Chris; Stimely, Laura, 2014, Tsunami impact to Washington and northern Oregon from segment ruptures on the southern Cascadia subduction zone: Natural Hazards, v. 72, no. 2, p. 849–870. [https://doi.org/10.1007/s11069-014-1041-7]

Satake, Kenji; Shimazaki, Kunihiko; Tsuji, Yoshinobu; Ueda, Kazue, 1996, Time and size of a giant earthquake in Cascadia inferred from Japanese tsunami records of January 1700: Nature, v. 379, no. 6562, p. 246–249. [https://doi.org/10.1038/379246a0]

Satake, Kenji; Wang, Kelin; Atwater, B. F., 2003, Fault slip and seismic moment of the 1700 Cascadia earthquake inferred from Japanese tsunami descriptions: Journal of Geophysical Research, v. 108, no. B11, 17 p. [https://doi.org/10.1029/2003JB002521]

Synolakis, C. E.; Bernard, E. N.; Titov, V. V.; Kânoğlu, Utku; González, F. I., 2007, Standards, criteria, and procedures for NOAA evaluation of tsunami numerical models: National Oceanic and Atmospheric Administration Technical Memorandum OAR PMEL-135, 60 p. [https://repository.library.noaa.gov/view/noaa/11073/noaa_11073_DS1.pdf]

Tadepelli, Srinivas; Synolakis, C. E., 1994, The run-up of N-waves on sloping beaches: Proceedings of the Royal Society of London A, v. 445, no. 1923, p. 99–112. [https://doi.org/10.1098/rspa.1994.0050]

Titov, V. V.; Arcas, Diego; Moore, C. W.; LeVeque, R. J.; Adams, L. M.; González, F. I., 2018, Tsunami hazard assessment of Bainbridge Island, Washington Project Report: Washington State Emergency Management Division, 43 p. [http://depts.washington.edu/ptha/WA_EMD_Bainbridge/BainbridgeIslandTHA.pdf].

Titov, V. V.; Kânoğlu, Utku; Synolakis, C. E., 2016, Development of MOST for real-time tsunami forecasting: Journal of Waterway, Port, Coastal, and Ocean Engineering, v. 142, no. 6, 48 p. [https://doi.org/10.1061/(ASCE)WW.1943-5460.0000357]

Titov, V. V.; González, F. I., 1997, Implementation and testing of the Method of Splitting Tsunami (MOST) model: NOAA Technical Memorandum ERL PMEL-112, 11 p. [https://www.pmel.noaa.gov/pubs/PDF/tito1927/tito1927.pdf]

Titov, V. V.; Synolakis, C. E., 1995, Modeling of breaking and nonbreaking long-wave evolution and runup using VTCS-2: Journal of Waterway, Port, Coastal, and Ocean Engineering, v. 121, no. 6, p. 308–316.

Titov, V. V.; Synolakis, C. E., 1998, Numerical modeling of tidal wave runup: Journal of Waterway, Port, Coastal, and Ocean Engineering, v. 124, no. 4, p. 157–171. [https://doi.org/10.1061/(ASCE)0733-950X(1998)124:4(157)]

Walsh, T. J.; Arcas, Diego; Titov, V. V.; Chamberlin, C. C., 2014, Tsunami hazard map of Everett, Washington: Model results for magnitude 7.3 and 6.7 Seattle fault earthquakes: Washington Division of Geology and Earth Resources Open File Report 2014-03, 1 plate, scale 1:32,000. [http://www.dnr.wa.gov/publications/ger_ofr2014-03_tsunami_hazard_everett.pdf]

Walsh, T. J.; Arcas, Diego; Venturato, A. J.; Titov, V. V.; Mofjeld, H. O.; Chamberlin, C. C.; González, F. I., 2009, Tsunami hazard map of Tacoma, Washington—Model results for Seattle fault and Tacoma fault earthquake tsunamis: Washington Division of Geology and Earth Resources Open File Report 2009-9, 1 sheet, scale 1:24,000. [http://www.dnr.wa.gov/publications/ger_ofr2009-9_tsunami_hazard_tacoma.pdf]

Walsh, T. J.; Caruthers, C. G.; Heinitz, A. C.; Myers, E. P., III; Baptista, A. M.; Erdakos, G. B.; Kamphaus, R. A., 2000, Tsunami hazard map of the southern Washington coast—Modeled tsunami inundation from a Cascadia subduction zone earthquake: Washington Division of Geology and Earth Resources Geologic Map GM-49, 1 sheet, scale 1:100,000, with 12 p. text. [http://www.dnr.wa.gov/publications/ger_gm49_tsunami_hazard_southern_coast.zip]

Walsh, T. J.; Gica, Edison; Arcas, Diego; Titov, V. V.; Eungard, D. W., 2016, Tsunami hazard maps of the San Juan Islands, Washington—Model results from a Cascadia subduction zone earthquake scenario: Washington Division of Geology and Earth Resources Map Series 2016-01, 4 sheets, scale 1:24,000 and 1:48,000, 9 p. text. [http://www.dnr.wa.gov/publications/ger_ms2016-01_tsunami_hazard_san_juan_islands.zip]

Walsh, T. J.; Myers, E. P., III; Baptista, A. M., 2002a, Tsunami inundation map of the Port Angeles, Washington area: Washington Division of Geology and Earth Resources Open File Report 2002-1, 1 sheet, scale 1:24,000. [http://www.dnr.wa.gov/publications/ger_ofr2002-1_tsunami_hazard_portangeles.pdf]

Walsh, T. J.; Myers, E. P., III; Baptista, A. M., 2002b, Tsunami inundation map of the Port Townsend, Washington area: Washington Division of Geology and Earth Resources Open File Report 2002-2, 1 sheet, scale 1:24,000. [http://www.dnr.wa.gov/publications/ger_ofr2002-2_tsunami_hazard_porttownsend.pdf]

Walsh, T. J.; Myers, E. P., III; Baptista, A. M., 2003a, Tsunami inundation map of the Neah Bay, Washington, area: Washington Division of Geology and Earth Resources Open File Report 2003-2, 1 sheet, scale 1:24,000. [http://www.dnr.wa.gov/publications/ger_ofr2003-2_tsunami_hazard_neahbay.pdf]

Walsh, T. J.; Myers, E. P., III; Baptista, A. M., 2003b, Tsunami inundation map of the Quileute, Washington, area: Washington Division of Geology and Earth Resources Open File Report 2003-1, 1 sheet, scale 1:24,000. [http://www.dnr.wa.gov/publications/ger_ofr2003-1_tsunami_hazard_quileute.pdf]

Walsh, T. J.; Titov, V. V.; Venturato, A. J.; Mofjeld, H. O.; González, F. I., 2003c, Tsunami hazard map of the Elliott Bay area, Seattle, Washington—Modeled tsunami inundation from a Seattle Fault earthquake: Washington Division of Geology and Earth Resources Open File Report 2003-14, 1 sheet, scale 1:50,000. [http://www.dnr.wa.gov/publications/ger_ofr2003-14_tsunami_hazard_elliottbay.pdf]

Walsh, T. J.; Titov, V. V.; Venturato, A. J.; Mofjeld, H. O.; González, F. I., 2004, Tsunami hazard map of the Bellingham area, Washington—Modeled tsunami inundation from a Cascadia subduction zone earthquake: Washington Division of Geology and Earth Resources Open File Report 2004-15, 1 sheet, scale 1:50,000. [http://www.dnr.wa.gov/publications/ger_ofr2004-15_tsunami_hazard_bellingham.pdf]

Walsh, T. J.; Titov, V. V.; Venturato, A. J.; Mofjeld, H. O.; González, F. I., 2005, Tsunami hazard map of the Anacortes-Whidbey Island area, Washington—Modeled tsunami inundation from a Cascadia subduction zone earthquake: Washington Division of Geology and Earth Resources Open File Report 2005-1, 1 sheet, scale 1:62,500. [http://www.dnr.wa.gov/publications/ger_ofr2005-1_tsunami_hazard_anacortes_whidbey.pdf]

Wang, Kelin; Tréhu, A. M., 2016, Invited review paper: Some outstanding issues in the study of great megathrust earthquakes—The Cascadia example: Journal of Geodynamics, v. 98, p. 1–18. [https://doi.org/10.1016/j.jog.2016.03.010]

Wang, P.-L.; Engelhart, S. E.; Wang, Kelin; Hawkes, A. D.; Horton, B. P.; Nelson, A. R.; Witter, R. C., 2013, Heterogeneous rupture in the great Cascadia earthquake of 1700 inferred from coastal subsidence estimates: Journal of Geophysical Research, v. 118, no. 5, p. 2460–2473. [https://doi.org/10.1002/jgrb.50101]

Williams, H. F. L.; Hutchinson, Ian, 2000, Stratigraphic and microfossil evidence for late Holocene tsunamis at Swantown Marsh, Whidbey Island, Washington: Quaternary Research, v. 54, no. 2, p. 218–227. [https://doi.org/10.1006/qres.2000.2162]

Williams, H. F. L.; Hutchinson, Ian; Nelson, A. R., 2005, Multiple sources for late-Holocene tsunamis at Discovery Bay, Washington State, USA: The Holocene, v. 15, no. 1, p. 60–73. [https://doi.org/10.1191/0956683605hl784rp]

Witter, R. C.; Kelsey, H. M.; Hemphill-Haley, Eileen, 2003, Great Cascadia earthquakes and tsunamis of the past 6700 years, Coquille River estuary, southern coastal Oregon: Geological Society of America Bulletin, v. 115, no. 10, p. 1289–1306. [https://doi.org/10.1130/B25189.1]

Witter, R. C.; Zhang, Y. J.; Wang, Kelin; Goldfinger, Chris; Priest, G. R.; Allan, J. C., 2012, Coseismic slip on the southern Cascadia megathrust implied by tsunami deposits in an Oregon lake and earthquake-triggered marine turbidites: Journal of Geophysical Research, v. 117, no. B10, 17 p. [https://doi.org/10.1029/2012JB009404]

Witter, R. C.; Zhang, Y. J.; Wang, Kelin; Priest, G. R.; Goldfinger, Chris; Stimely, L. L.; English, J. T.; Ferro, P. A., 2011, Simulating tsunami inundation at Bandon, Coos County, Oregon, using hypothetical Cascadia and Alaska earthquake scenarios: Oregon Department of Geology and Mineral Industries Special Paper 43, 57 p. [http://www.oregongeology.org/pubs/sp/p-SP-43.htm]

Witter, R. C.; Zhang, Y. J.; Wang, Kelin; Priest, G. R.; Goldfinger, Chris; Stimely, Laura; English, J. T.; Ferro, P. A., 2013, Simulated tsunami inundation for a range of Cascadia megathrust earthquake scenarios at Bandon, Oregon, USA: Geosphere, v. 9, no. 6, p. 1783–1803. [https://doi.org/10.1130/GES00899.1]

Yamaguchi, D. K.; Atwater, B. F.; Bunker, D. E.; Benson, B. E.; Reid, M. S., 1997, Tree-ring dating the 1700 Cascadia earthquake: Nature, v. 389, p. 922–923. [https://doi.org/10.1038/40048]

Zhang, Y. J.; Witter, R. C.; Priest, G. R., 2011, Tsunami-tide interaction in 1964 Prince William Sound tsunami: Ocean Modelling, v. 40, no. 3–4, p. 246–259. [https://doi.org/10.1016/j.ocemod.2011.09.005]

Appendix A. Tsunami Source Evidence and Models

Applying evidence of past tsunamis is the best way to prepare for future tsunamis. One important piece of geologic evidence for past tsunamis is the deposits they leave behind. Tsunami deposits are typically preserved in tidal-marsh stratigraphy and consist of normally graded sand beds that may contain marine microfossils (Morton and others, 2007). There are many locations containing tsunami deposits within Washington, mostly preserved along the Pacific coast, which suggests a nearby source like the Cascadia subduction zone (CSZ; Peters and others, 2003). Researchers have also found tsunami deposits within Washington's inner waterways that correlate to the same approximate timing as the outer coast deposits, indicating that the CSZ is capable of producing powerful tsunamis that penetrate into the Salish Sea. These locations include the Strait of Juan de Fuca at Salt Creek (Hutchinson and others, 2013), Discovery Bay (near Port Townsend; Williams and others, 2005), the west shore of Whidbey Island (Fig. 2; Williams and Hutchison, 2000), and as far south as Lynch Cove at the terminus of Hood Canal (Discovery Bay stratigraphy interpreted in Fig. A1; Garrison-Laney, 2017).

This appendix reviews past evidence for earthquakes and their resultant tsunamis that have impacted Washington's inner and outer coastlines. This includes a discussion of evidence

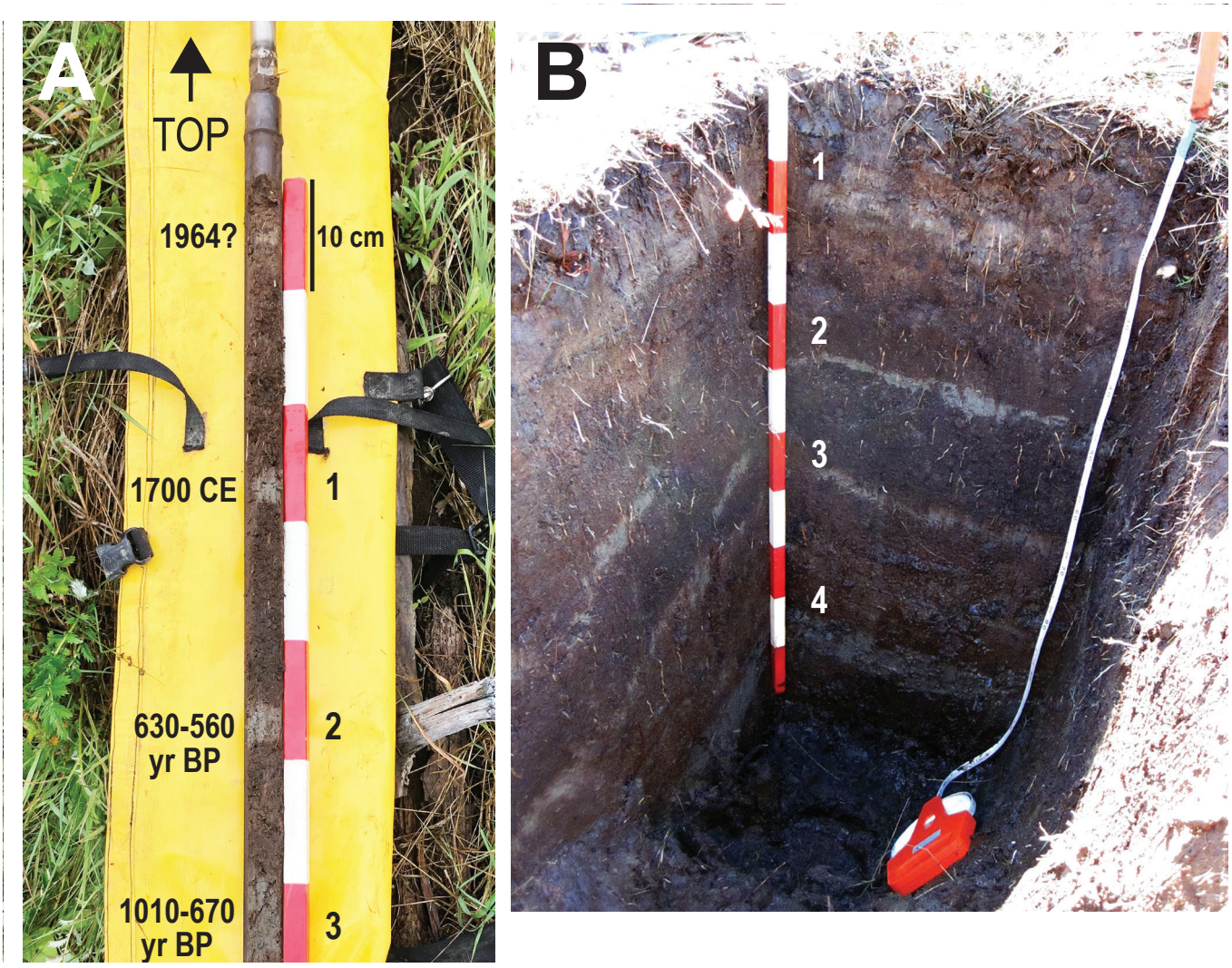

Figure A1. Tsunami deposits at Discovery Bay, Washington. The characteristics of Discovery Bay, including its tapering shape, tidal marsh at the head of the bay, and slow tidal currents, create a setting that has preserved at least nine deposits in the last 2,500 years (Williams and others, 2005). **A.** A gouge core with tsunami deposits (lighter colored layers) interbedded with tidal marsh peat. The tsunami deposits are sand and silt layers that were deposited on top of the tidal marsh, eventually to be covered by new tidal marsh plants. Tsunami deposits numbered 1–4 are presumed to be from Cascadia earthquake-generated tsunamis, although other sources are possible. Deposit 1 is presumed to be from the most recent Cascadia earthquake in 1700 CE. Near the top of the core is a thinner deposit that may be from the 1964 Alaskan tsunami. The tidal marsh and a nearby residence were flooded by the 1964 tsunami. The age of each layer is shown in yr BP, or "years before present," and were obtained from radiocarbon dating of plant remains (Williams and others, 2005; Garrison-Laney and Miller, 2017). **B.** A pit dug into the surface of the tidal marsh near the location of the core in A shows the same stratigraphy. The red and white stick is 1 meter (3 feet) long, painted in 10 cm increments. Photos taken by Carrie Garrison-Laney, Washington Sea Grant.

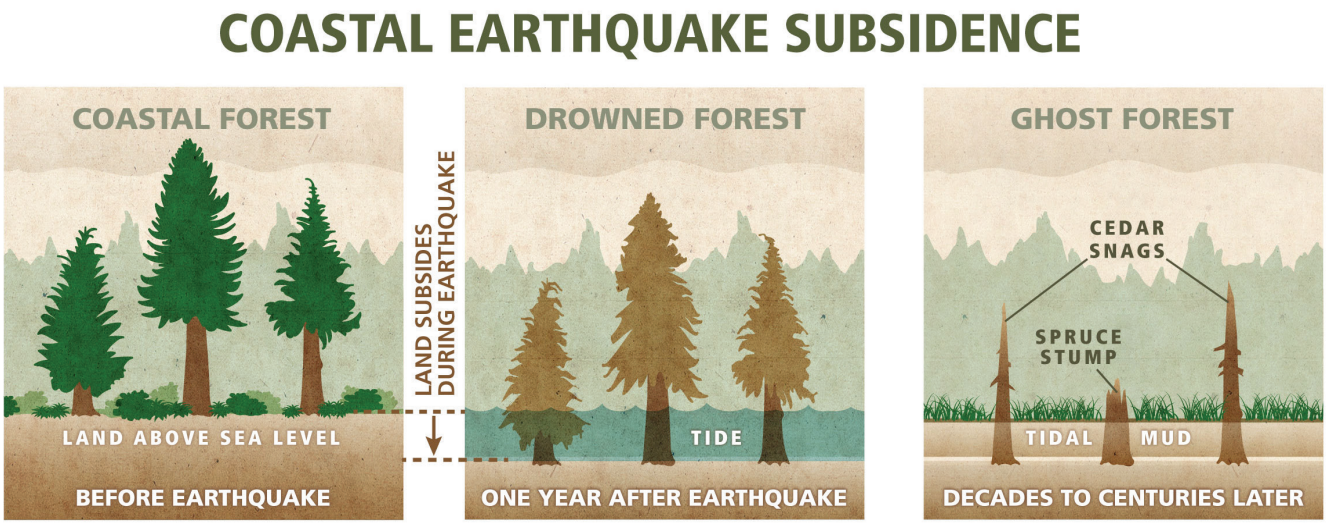

Figure A2. Schematic showing the formation of ghost forests over time as described in Atwater and Yamaguchi (1991), Atwater (1992), and Atwater and others (1995; 2005). Trees that were once above sea level may subside to below the tidal level following an earthquake. These trees die by saltwater intrusion, leaving behind distinctive cedar snags seen in coastal and tidal areas (spruce stumps shown here are exaggerated and are not typically seen protruding through tidal mud). Dendrochronology techniques can reveal when the sudden subsidence occurred. Between earthquake events, the land level slowly rebounds to elevations similar to pre-earthquake conditions (the land may not recover all elastic deformation) and a forest once again grows. This cycle then repeats itself following the next earthquake event.

from the geologic record that was used to calculate recurrence intervals for the CSZ (the frequency of how often earthquakes occur). Recurrence intervals and the characterization of past tsunamis come from many lines of evidence, including coastal earthquake subsidence, tsunami deposits, deep-sea sediment cores, marine microfossils (diatoms), and oral and written histories. All of this evidence points to numerous earthquakes and tsunamis that originated from the CSZ, and researchers believe that Washington has experienced both moderate to large tsunamis in the past.

REVIEW OF EVIDENCE

Coastal Earthquake Subsidence

Great subduction zone earthquakes commonly cause coincident land-level changes, known as coseismic subsidence and uplift (Plafker, 1969; Plafker and Savage, 1970). Coastal subsidence during great earthquakes causes sudden sea-level rise and drops salt marshes and uplands into lower intertidal environments; the sudden submergence is recorded geologically by stratigraphic sequences that show sharp contacts between buried marsh peat or upland soil and overlying estuarine mud (Atwater, 1992). Some coastal regions such as the banks of the Copalis River in southwest Washington also contain "ghost forests," or dead standing trees and other vegetation that were suddenly submerged in seawater (Fig. A2; Atwater, 1992). Dendrochronology and radiocarbon dating techniques reveal when these submergence events occurred and allow for reconstructions of past great earthquake events (Jacoby and others, 1997; Yamaguchi and others, 1997). Atwater and Hemphill-Haley (1997) reported six sudden submergence events in Willapa Bay over the last 3,500 years. Their data imply an average recurrence interval of about 520 years for earthquakes on the CSZ. However, individual intervals for each earthquake have varied between ~100 and ~1,300 years (Atwater and Hemphill-Haley, 1997).

Tsunami Deposits

Researchers working in Oregon have found a somewhat different record farther south. Using marsh stratigraphy and inferred tsunami deposits, Kelsey and others (2002) found a 5,500-year record of 11 earthquake events at Sixes River in southern Oregon. These records also include an abrupt subsidence event not observed on the southern Washington coast. Kelsey and others (2005) examined Bradley Lake on the southern Oregon coast near Bandon and found that it included probable tsunami deposits with an average recurrence interval of ~390 years. The shorter recurrence interval in southern Oregon implies that some earthquakes on the CSZ did not produce abrupt subsidence in southern Washington. A possible explanation is that the CSZ earthquakes recorded in Oregon did not rupture the entire length of the subduction zone, resulting in a spatially heterogeneous response in the geologic record. Nelson and others (2006) examined the degree of overlap and amount of abrupt subsidence at eight sites along the Oregon and Washington coasts. They concluded that rupture area (and therefore earthquake magnitudes) varied—ruptures along the northern CSZ are generally longer, whereas ruptures along the southern CSZ are more variable in both length and recurrence interval.

Deep-Sea Sediment Cores

Another approach to inferring recurrence intervals is the correlation of turbidites—deposits of sediment gravity flows, or turbidity currents—out on the abyssal plain (Griggs and Kulm, 1970). Adams (1990) inferred that great earthquakes triggered turbidity currents in Cascadia Channel and Astoria Canyon (Fig. A3). Oregon State University researchers logged

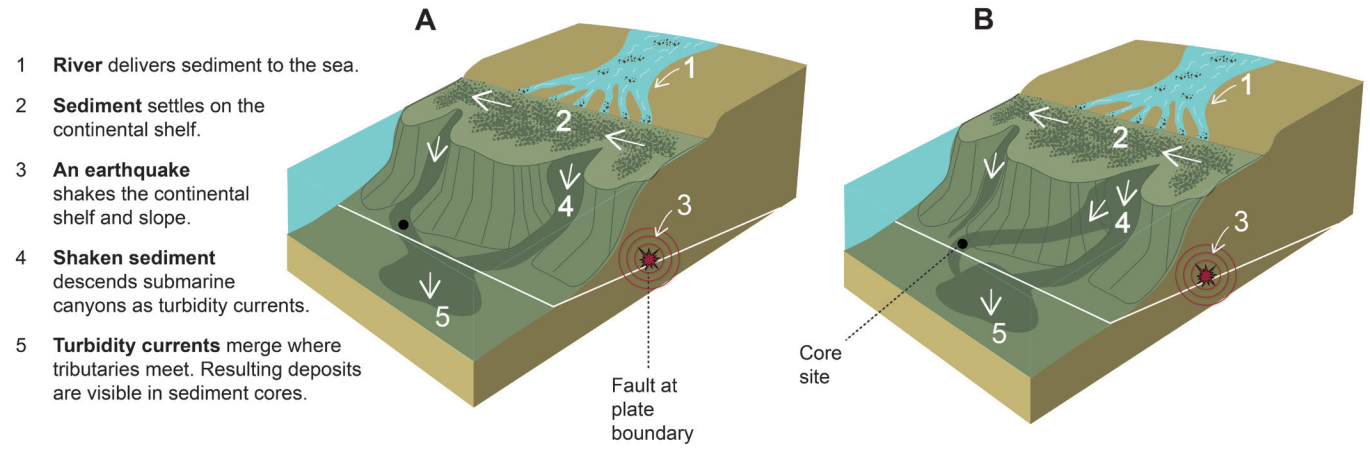

Figure A3. Two alternative schematic views of turbidity currents descending submarine canyons. **A.** Turbidity current flows produced by seismic shaking (modified from Adams; 1990). Extensive shaking enables turbidity currents to descend different submarine channels at the same time and merge. **B**. Turbidity current flows influenced more by differences in sediment supply than by seismic shaking (modified from Atwater and others; 2014). Turbidite stratigraphy at a specific core site at one submarine canyon may suggest that accumulation occurs by way of latitudinal spillover from other submarine canyons with differing sediment supply to canyon heads. In this case, shaking from the upper canyon shown may also have limited sediment supply and produce few, if any turbidity currents before merging where the tributaries meet. These contrasting views require future research focused on sediment supply, flow initiations, and downstream pathways.

Table A1. Estimates of earthquake recurrence on the Cascadia subduction zone.

Events over time interval	Average recurrence interval in years; range if given	Section of CSZ	Reference	Major evidence
6 submergence events in 3,500 years	500–540 average, 100–300 to 1,300	northern	Atwater and Hemphill-Haley (1997)	submergence events
11 submergence events in 5,500 years	510	southern	Kelsey and others (2002)	marsh stratigraphy and tsunami deposits
13 tsunami deposits, 17 disturbances in 7,000 years	390 average for local tsunamis entering Bradley Lake; ~500 year average for ruptures along the southern margin	southern	Kelsey and others (2005)	marine incursions and disturbance events in Bradley Lake
13 turbidites post Mazama ash (6,845 years BP [calibrated to ~7,700 cal yr BP])	590 ±170	northern	Adams (1990)	turbidites in Astoria Canyon and Cascadia Channel
19 or 20 full-margin turbidites in 10,000 years; 22 turbidites restricted to the south	500–530 average for full-margin rupture, ~240 full-margin plus southern only	whole and partial	Goldfinger and others (2012)	turbidites along Cascadia margin
20 full-margin turbidites in 10,000 years; 3 turbidites on a segment running from northern California to Juan de Fuca Channel; 1 turbidite off Washington and British Columbia only	500–530 average for full-margin rupture; ~434 full-margin plus shorter ruptures adjacent to Washington	whole and partial	Goldfinger and others (2017)	turbidites along Cascadia margin

13 turbidites in both Cascadia Channel and Astoria Canyon from multiple deep-sea cores, suggesting 13 CSZ ruptures (Griggs, 1968; Adams, 1990). All 13 turbidite deposits were located stratigraphically above the Mazama ash (erupted from Mount Mazama volcano), implying that they are younger than the Mazama ash. Radiometric dating of the Mazama ash suggests an age of 6,845 ±50 radiocarbon years before present (BP; Adams, 1990). These findings indicate that earthquakes on the CSZ have an average recurrence interval of 590 ±170 years (Table A1; Adams, 1990).

Goldfinger and others (2012) supplemented Griggs' (1968) turbidite data that Adams (1990) correlated to the CSZ by collecting numerous additional cores in the seafloor along the Cascadia continental margin. From this updated record, Goldfinger and others (2012) concluded that the CSZ is capable of both full-length and partial ruptures of different sizes. They proposed that full-length ruptures offshore of northern California to British Columbia have a recurrence interval of 500 to 530 years, similar to the previous estimates of Adams (1990), Atwater (1992), and Atwater and Hemphill-Haley (1997).

Goldfinger and others (2012) additionally estimated a recurrence interval of ~240 years for partial ruptures, which include earthquakes offshore of Oregon and northern California.

Earthquakes that rupture only the northern part of the CSZ (including Washington) are also a possibility. Goldfinger and others (2017) selected additional sites for coring and seismic assessment offshore of the Washington continental shelf. Results from these new sites suggested a slight revision of their CSZ rupture model, extending several rupture boundaries from central Oregon farther north to include southwest Washington. They also inferred an additional event offshore of Washington and southern British Columbia only, although their revision may still require further data collection. As a result, these findings led to minor variations in their interpretation on CSZ recurrence intervals. In their updated interpretation, recurrence for most of the Washington coast decreased to 434 years, with the exception of the northernmost section (possible recurrence interval of 430–500 years) where turbidites of recent millennia are inconspicuous or absent (Goldfinger and others, 2017). This proposed change in interpretation suggests that there is a 10–17 percent chance that Washington experiences a CSZ earthquake within the next 50 years (probability estimate based off Gaussian and log-normal time-dependent distributions; Goldfinger and others, 2017). However, Atwater and others (2014) argued that the absence of core data and turbidites along the northern CSZ does not necessarily disprove ground shaking. Differences in sediment supply and flow paths down tributary channels may prohibit turbidites in this section of the CSZ (Fig. A3). Atwater and others (2014) further questioned the rupture lengths proposed by Goldfinger and others (2012). These rupture lengths were determined based on age correlations of widely spaced core sites, but the ages of each core site could not always be adequately determined.

Diatoms

Further studies on Discovery Bay, located on the northeast part of the Olympic Peninsula, detected nine muddy sand beds bearing marine microfossils (diatoms) that interrupt a 2,500-year-old sequence of peat deposits beneath a tidal marsh (Williams and others, 2005). Diatoms can assist in characterizing past earthquake events and are a useful proxy for land level and sea level change over time. This is because different species of diatoms occupy diverse environmental niches, and researchers can use any changes in diatom assemblages over time to infer changes in the coastal environment. The ages of four of these beds, more precisely determined by Garrison-Laney and Miller (2017), overlap with inferred late-Holocene tsunamis generated by full-length ruptures of the CSZ (Goldfinger and others, 2012). Diatoms found in peat deposits bracketing these four beds do not indicate a concurrent change in sea level and elevation at Discovery Bay. This suggests that CSZ-associated coseismic subsidence has been negligible as far east as Discovery Bay. Other sand sheets in the sequence may represent tsunamis generated by partial ruptures of the CSZ, by upper plate fault earthquakes, or by landslides (Garrison-Laney and Miller, 2017), none of which triggered turbidity currents. This implies either that some CSZ earthquakes do not leave turbidite deposits in Cascadia Channel (Atwater and others, 2014), or that other events such as local earthquakes or landslides generated some tsunami deposits, both of which are plausible.

Oral and Written Histories

Subduction zone earthquakes can generate tsunamis that are capable of crossing oceans. A key historical component of documenting the timing of the last CSZ-induced tsunami comes from historical reports in Japan. According to the Japanese record, accounts of unusual seas, flooded fields, damaged property, and damaged freight were reported on January 27 and 28, 1700. Although there was abnormal flooding in Japan's coastal areas, some writers and diarists were resistant to call it a tsunami because they did not feel earthquake shaking. Instead, the Mayor of Tanabe had reported on "unusual seas" and the scribe for the town of Ōtsuchi called it a "high tide" (Atwater and others, 2005; Henderson, 2014). Abnormal flooding events had occurred many other times in Japan, though researchers were able to attribute them to other locations of known distant earthquakes, such as South America. Uniquely, the event in 1700 later became known as the "orphan tsunami" (Atwater and others, 2005) because it lacked an apparent earthquake source. On the other side of the Pacific Ocean, histories passed down through native oral storytelling also mention powerful waves and shaking throughout the Pacific Northwest around this time (Ludwin, 2002). For example, Heaton and Snavely (1985) reported that Makah Tribal histories describe what could be a tsunami flowing through Waatch Prairie near Cape Flattery (Fig. 2).

EARTHQUAKE SLIP DISTRIBUTIONS AND TSUNAMI MODELS

1700 Earthquake

Nearly 300 years passed before researchers attributed the flooding that occurred in 1700 in Japan to possible fault activity within the CSZ (Satake and others, 1996). Satake and others (2003) tested various possible rupture dimensions and slip amounts to match the observed tsunami wave heights recorded in Japan. They assumed that this event ruptured the full 684 mi (~1,100 km; Flück and others, 1997) length of the CSZ and inferred 62 ft (19 m) of uniform, coseismic slip within the full-slip zone. The average slip over the whole subduction zone, including the full-slip and down-dip partial slip zone, equaled 46 ft (14 m), suggesting a magnitude of 8.7 to 9.2 (Satake and others, 2003). They inferred that the most likely magnitude was 9.0 based on the correlation between estimates of coseismic subsidence from paleoseismic studies and the subsidence predicted by their models.

While these early rupture models assumed a uniform slip distribution along the megathrust, all instrumentally recorded subduction zone earthquakes ruptured heterogeneously (for example, 2004 Sumatra, 2010 Chile, and 2011 Japan). Wang and others (2013) developed a heterogeneous earthquake deformation scenario for the 1700 CSZ earthquake. Their models allow slip to vary both along strike and in the dip direction, which correlates with the more precise estimates of subsidence and uplift constrained by detailed tidal microfossil studies than the uniform slip models. Better estimates of paleoseismic deformation are useful for delineating future earthquake and tsunami behavior,

but a heterogeneous slip distribution is challenging to predict and model.

Pre-1700 Earthquakes

PARTIAL-LENGTH RUPTURE MODELS

The magnitudes and slip distributions of earlier CSZ earthquakes are not as well constrained. Inferences of shorter ruptures that affect only the southern part of the CSZ generally imply smaller magnitude earthquakes. Priest and others (2014) modeled tsunamis from several postulated shorter ruptures limited to the southern part of the CSZ and concluded that the tsunamis they generated were significantly smaller in Washington than those generated by full-length ruptures. A partial CSZ rupture restricted to the north was suggested by Goldfinger and others (2013) and Peterson and others (2013). Goldfinger and others (2017) later substantiated this northern rupture, but there is insufficient paleoseismic data to generate a tsunami model (see figs. 9 and 18 in Goldfinger and others, 2017). Therefore, the study presented here does not consider these smaller events.

FULL-LENGTH RUPTURE MODELS

Witter and others (2012) hypothesized that the earthquakes generated by the CSZ over the last 10,000 years have been highly variable, with some larger than the last one in the year 1700. This deduction comes from synthesizing multiple data including: (1) the turbidite data from Goldfinger and others (2012); (2) the correlation of inferred tsunami deposits with turbidites in Bradley Lake, Oregon (Witter and others, 2012); and (3) interpretation of tsunami deposits in the Coquille River estuary at Bandon, Oregon that extend as much as 6.2 mi (10 km) farther inland than the tsunami deposits from the 1700 event (Witter and others, 2003). Previously, Witter and others (2011) constructed 15 scenarios of full-length ruptures where they adjusted vertical seafloor deformation to simulate tsunami differences in inundation at Bandon, Oregon. These rupture scenarios included slip partitioned to a splay fault in the accretionary wedge as well as scenarios that varied the up-dip limit of slip on a buried megathrust fault. In tsunami modeling, the water column moves as an incompressible fluid, suggesting that any seafloor deformation will directly influence tsunami generation (Berger and others, 2011). Since splay fault ruptures breach the seafloor directly, they consequently could generate larger tsunamis than other types of earthquakes buried on the megathrust that do not and only cause seafloor deformation through elastic deformation of the upper plate. Thus, modeling a splay fault rupture effectively boosts tsunami generation. However, researchers have not decisively confirmed the existence of a splay fault in the CSZ, although some indirect structural evidence hints at this possibility on parts of the margin (Wang and Tréhu, 2016). To assess these rupture scenarios, Witter and others (2011, 2012) performed numerical tsunami simulations for Bradley Lake and Bandon. They used a logic tree approach to rank model consistency by comparing the results of each simulation with geophysical and geological data from the distribution of inferred tsunami deposits. Witter and others (2011) found that the observational tsunami data were broadly compatible with their larger scenarios.

Of the 15 CSZ scenarios modeled by Witter and others (2011), scenario L1—a splay fault model with a maximum slip of 88.6 ft (27 m) and an average slip of 42.6 ft (13 m)—produced a tsunami that encompassed 95 percent of the variability in their simulations. In other words, the L1 scenario produces tsunami inundation as extensive as, or more extensive than most (95 percent) other models along the Oregon coast. We have inferred these model results to be the same for the Puget Sound (disregarding potential tsunamis from crustal fault or landslide sources). Witter and others (2011) tied the assumed rate of plate convergence to the existing turbidite paleoseismic records (Goldfinger and others, 2012). They did this to estimate the size of the earthquakes that generated the turbidites, which were assigned to 19 stratigraphic units. However, Goldfinger and others (2012) debatably correlated these units among widely separated cores along the full length of the CSZ margin. These earthquake sizes were further constrained from tsunami simulations at Bradley Lake, Oregon (Witter and others, 2013). They concluded that three earthquakes in the last ~10,000 years were probably similar to scenario ‘L’ and only one was larger (table 1 in Witter and others, 2011). The intervals between the inferred ‘L’ and larger earthquakes are ~1,800 to ~4,600 years apart. Another way to estimate recurrence frequency is that if four earthquakes in the last 10,000 years are ‘L’ or larger, then these types of events have an average recurrence interval between 2,500 and 5,000 years.

Witter and others (2011) recommended considering the L1 scenario for land-use planning and revisions to coastal building codes. If the L1 scenario represents 95 percent of the hazard over a 10,000-year period, then scenario ‘L’ earthquakes have a long recurrence interval with a probability of occurrence that is on the same order as the International Building Code (seismic standard of 2 percent probability of exceedance in 50 years; International Code Council, 2015). Much of the geological evidence presented in this publication that justifies the use of the (Extended) L1 scenario, such as the turbidite record and tsunami deposits, have also been included in efforts to create the United States Geological Survey (USGS) national seismic hazard maps (Petersen and others, 2014).